NOTE TO USERS

Design and Fabrication of a Micromachined Tactile Sensor for Endoscopic Graspers

Nakka Purushotham Rao

A Thesis

in

The Department

of

Mechanical and Industrial Engineering

Presented in Partial Fulfillment of the Requirements

for the degree of Master of Applied Science at

Concordia University

Montreal, Quebec, Canada.

October 2004

ABSTRACT

Design and Fabrication of a Micromachined Tactile Sensor for Endoscopic Graspers

Purushotham Rao Nakka

The present day endoscopic graspers are designed to be tooth-like in order to grasp slippery tissue during Minimally Invasive Surgery (MIS). However they do not have any sensing device to provide the surgeons any tactile feedback. This thesis describes the design, fabrication and testing of a micro-machined tooth-like tactile sensor, which can be integrated with the tip of an endoscopic grasper.

The sensor consists of three parts; the first part is a 25-micron polyvinylidene fluoride (PVDF) film. The second part is made of a silicon substrate with cavities etched using anisotropic etching of silicon. The bottoms of the cavities are covered with a layer of aluminum. The two parts then are bond to each other in such a way that the lower aluminum layer of PVDF is facing the bottom of the cavities forming a parallel plate capacitor with the aluminum layer in the cavity. The third layer is a 0.5mm thick tooth-like plexiglass glued on the top of the PVDF.

The static response of the sensor is obtained by applying a static force on the tooth and measuring the change in capacitance between the bottom electrode of the

PVDF film and the electrode deposited on surface of the etched cavity. The dynamic response of the device is determined by applying a sinusoidal force on the tooth of the sensor and measuring the output voltage from the PVDF film. The experimental results are compared with both analytical and finite element results. The sensor exhibits high sensitivity and linearity. The sensor can also be integrated with a commercial endoscopic grasper without changing its original design.

Dedicated To :

        My Parents, brother and sisters.

ACKNOWLEDGEMENTS

TABLE OF CONTENTS

List of Figures

List of Tables

List of Acronyms and Symbols

LVDT	Linear Variable Differential Transformer
MEMS	Micro Electro Mechanical Systems
MIS	Minimal Invasive Surgery
MR	Magnetoresistive
PVDF	Polyvinylidene Fluoride
PZT	Lead Zirconate Titanate
Q	Charge
ρ	Density
MST	Micro-systems Technology
IC	Integrated Circuit
SiO_2	Silicon dioxide
KOH	Potassium hydroxide
TMAH	Tri Methyl Ammonium Hydroxide
PR	Photoresist
$\delta(x)$	Deflection
W	Load applied
L	Length of membrane
x	Position of the membrane were deflection is find
I	Moment of Inertia
ξ	Permittivity of medium

d	Distance between the electrodes
A	Area of the electrode
[c]	Elasticity Matrix (N/m^2)
[e]	Piezoelectric Matrix at Constant Stress (C/m^2)
g_{31}, g_{32}, g_{33}	Piezo Coefficient Related to the Voltage (V-m/N)
e	Piezoelectric Coefficient (C/m^2)
W	Width of Piezoelectric crystal
E	Modulus of Elasticity
V	Voltage
{F}	Force Vector for System
{d}	Element Nodal Displacement Vector
{D}	Electric Flux Density (C/m^2)
{E}	Electric Field Vector (V/m)
{f}	Element Nodal Force Vector
{S}	Strain Vector (Dimensionless)
{T}	Stress Vector (N/m^2)
{U}	Displacement Vector for System
[k]	Element Stiffness Matrix
α	Pyroelectric Coefficient $(C/^{\circ}Cm^2)$
C	Capacitance
1-D, 2-D	One Dimensional, Two Dimensional
d_{31}, d_{32}, d_{33}	Piezoelectric conistant

CHAPTER - 1

TACTILE SENSING TECHNOLOGY

1.1 Introduction

Minimally Invasive Surgery (MIS) represents a revolution in surgical practice and technology. Open surgery requires the creation of large access wounds in order to expose the relevant anatomy, and allow room for manipulation; This results in extreme trauma, large scars and postoperative complications. MIS provides access to the operation site by endoscopic tools via small insertion, hence providing many advantages over conventional open surgery, including less tissue trauma, less scarring, and faster post-operative recovery time. Although the techniques vary from procedure to procedure and among different surgical subspecialties, all minimally invasive surgical procedures employ video cameras and lens systems to provide anatomic visualization within a region of the body. However MIS is technically difficult and poses an increased risk of surgical complications. This is largely due to the present state of surgical instrument design that falls far-short of the dexterity and sensitivity of the human hand [1]. Simple, long handled tools able to fit through the small incisions are used to grasp, cut, cauterize, and staple the tissue. Figure 1-1 shows an example of a typical minimally invasive grasper (manufactured by Karl Storz Gmbh & Co; Tuttlingen, Germany). The type and complexity of surgical procedures is fundamentally limited by the instrument technology. The primary problems in current MIS [2] are:

1) There is a discrepancy between tool tip motion observed via an endoscopic camera and the motion of the surgeon's hand. This is due to camera placement and the fulcrum effect caused by passing long handled instruments through a fixed incision point.
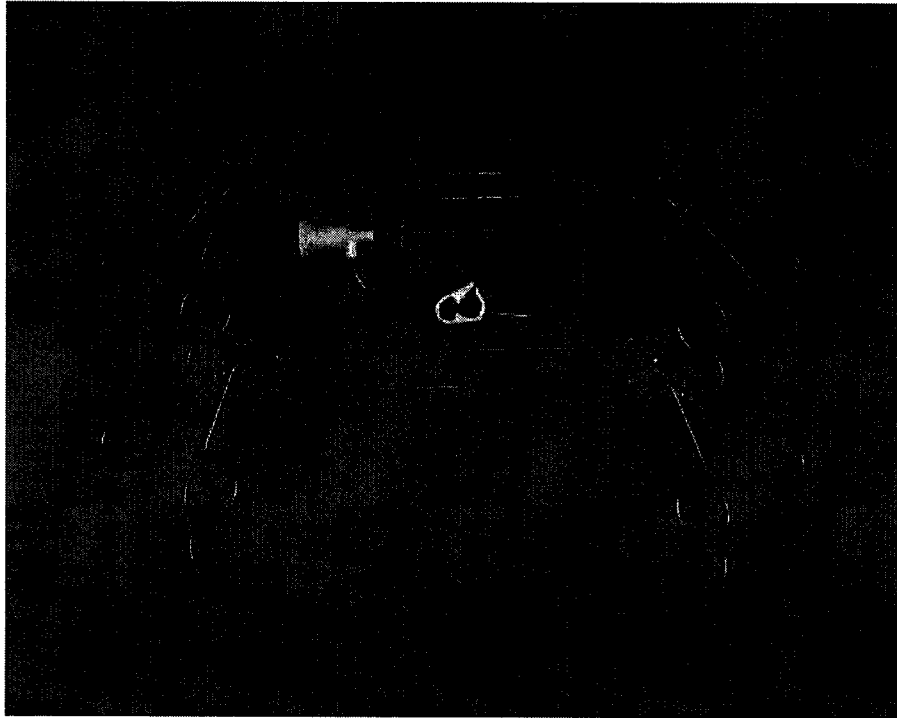
Figure 1-1. Typical Minimally Invasive tools. A rod running the length of the instrument shaft connects the motions of the scissors grip handle with the jaws of the gripper. Internal tisues are grasped by passing the instrument through a small incision in the patient's body. (Manufactured by Karl Storz GmbH & Co; Tuttlingen, Germany)

2) There is poor dexterity due to the lack of degrees-of-freedom in current MIS instruments, that limits tasks such as suturing and tying Knots.

3) There is a lack of force or tactile feedback to the surgeon through a long handled instrument [3], that is passed through a high friction air seal subjected to body wall disturbances.

2

Some of these problems have been addressed in previous systems. To make MIS more effective, surgeons should be able to feel the grasped tissue. This ability is particularly useful in situations where the grasped tissue is not in the surgeon's field of view [4-5]. The basic requirement for a competent tactile sensor is to determine the magnitude and the position of the force applied between the sensor and tissue (i.e. pressure distribution).

The field of integrated microsensors and microactuators, called "Micro-Electro-Mechanical Systems" (MEMS) or "Micro-Systems Technology" (MST), has made rapid strides in recent years [6-8], providing an important link between VLSI circuits and non-electronic monitoring and control applications. Microsystems merging electrical, mechanical, thermal, optical, magnetic, and chemical components are now being fabricated on a common substrate toward the development of high-performance closed-loop-controlled systems. Although a nascent technology, Minimally Invasive Surgery is now being preferred for many operative procedures. Despite its advantages, MIS dramatically reduces the surgeon's sensory perception during manipulation. Surgery is essentially a visual and tactile experience and any limitation on the surgeon's sensory abilities is undesirable.

In laparoscopy, long slender tools are inserted through small puncture openings in the abdominal wall and the surgeon uses a range of tip mounted instruments guided by video feedback images. As the instruments are rigid rods and effectively have fixed pivots at the entry points, the available degrees of freedom are restricted and therefore demand extra operator expertise. Voges [9] reports the main difficulties experienced in

3

the above mentioned procedure are to be: restricted manipulation mobility, lack of depth from 2D vision and the almost complete lack of a sense of touch. The relevance of tele-presence is clear and Voges predicts that future systems will have new designs of flexible instruments with greater mobility, 3D monitoring and data enhancement. It is clear that tactile sensing is greatly needed in this area and researchers are responding to the opportunity.

1.2 Technologies for Tactile Sensor

Many physical principles have been exploited in the development of tactile sensors. As the technologies involved are very diverse, this chapter considers only the generalities of the technology

involved. The development in tactile sensing technology is application driven and the operation of a tactile sensor is dependent on the material of the object being grasped.

1.2.1 Capacitive sensors

Capacitive sensors make use of the change in capacitance between two metal plates. The membrane deflects when pressure is applied, that causes the distance between the two electrodes to be changed. The capacitance change is measured and the pressure exerted can be calculated from membrane deflection. Despont et al. [10] had designed a silicon based capacitive pressure sensor. The electrodes in this are made of a planar comb structure. The sensor element comprised of two parts: first, a movable elastic structure that transforms a force into a displacement, and second, a transformation unit consisting

of electrodes that transform the displacement into a measurable change in capacitance. By separate measurement of the capacitance changes on both sides, high linearity and sensitivity were obtained. Compared to piezoresistive sensors, capacitive sensors have better long term stability, higher sensitivity and no hysteresis. However, the advantages of capacitive pressure sensors go along with more complex signal processing and higher production costs.

1.2.2 Conductive Elastomer sensor

Compliant materials that have a defined force resistance characteristic have received a lot of attention in tactile sensor research. The basic principle of conductive elastomer sensors lies in measuring the resistance of a conductive elastomer or foam between two points. The Majority of sensors use an elastomer that consists of a carbon-doped rubber. Figure 1-2 shows the schematic of a conductive elastomer sensor.

Applied Force

Increase in particle density

R1

R2
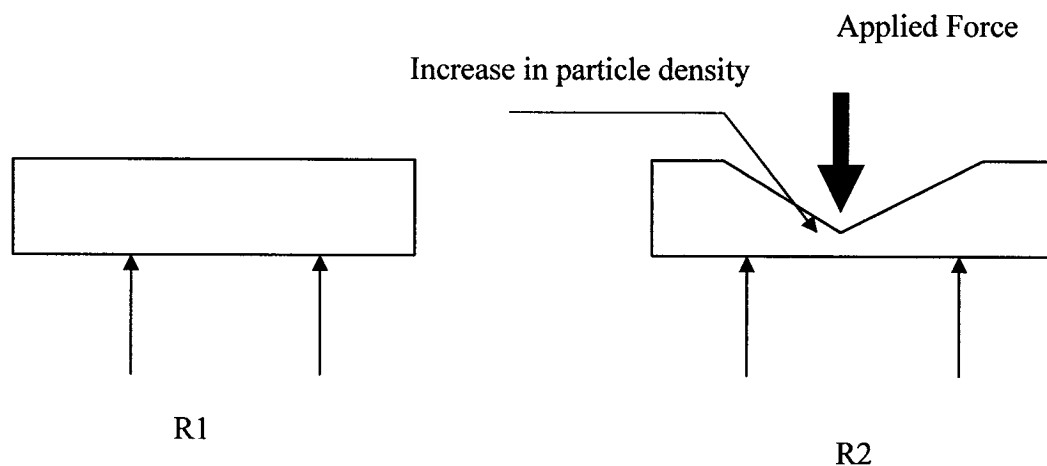
Figure 1-2. Schematic of a conductive elastomer sensor

In the above sensor, the resistance of elastomer changes with the application of force, resulting in the deformation of the elastomer, there by altering the particle density.

1.2.3 Magnetic based sensor

A magneto resistive or magneto elastic material is a material whose magnetic characteristics change with an externally applied physical force. Magneto elastic sensors have a number of advantages that include high sensitivity and dynamic range, no measurable mechanical hysteresis, a linear response, and physical robustness. Of the two approaches to designing tactile sensors based on magnetic transduction, the first one is based on the principle that the movement of a small magnet by an applied force will cause the flux density at the point of measurement to change. The observed change in flux density can then be measured using Hall effect or by a magneto resistive device. The second approach involves the fabrication of the core of a transformer or inductor from a magneto elastic material that will deform under pressure and cause the magnetic coupling between the transformer windings to change. If a very small permanent magnet is held

above the detection device by a complaint medium, the change in flux caused by the magnet's movement due to an applied force can be detected and measured. The field intensity follows an inverse relationship, leading to a nonlinear response, which can be easily linearized by processing. A tactile sensor using magneto elastic materials consists of material bonded to the substrate, and is used as a core for an inductor. As the core is stressed, the material's susceptibility changes, that is measured as a change in the coil's inductance.

6

1.2.4 Optical Sensors

The rapid expansion of optical technology in recent years has led to the development of a wide range of tactile sensors. The operating principles of optical-based sensors are well known and fall into two classes: Intrinsic, where the optical phase, intensity, or polarization of transmitted light are modulated without interrupting the optical path and Extrinsic, where the physical stimulus interacts with the light external to the primary light path.

Intrinsic and extrinsic optical sensors can be used for touch, torque, and force sensing. For industrial applications, the most suitable will be that which requires the least optical processing. For robotic touch and force-sensing applications, the extrinsic sensor based on intensity measurement is the most widely used due to its simplicity of construction and subsequent information processing.

Touch and tactile optical sensors have been developed using a range of optical technologies. The force sensitivity in the optical sensor is determined by a spring or elastomer. To prevent cross talk from external sources, the sensor can be constructed around a deformable tube, resulting in a highly compact sensor. A Schematic of an optical sensor is shown in Figure 1-3.
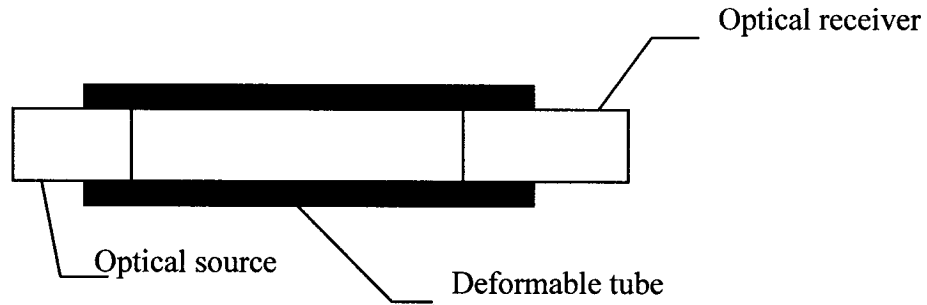
Figure 1-3. Optical Sensor

1.2.5 Strain Gauge Sensor

Strain is the amount of deformation undergone by a body due to an applied force. More specifically, strain (ε) is defined as the fractional change in length. There are several methods of measuring strain, the most common being the use of a strain gauge, a device whose electrical resistance varies in proportion to the amount of strain in the device. The most widely used gauge is the bonded metallic strain gauge. The metallic strain gauge consists of a very fine wire or, metallic foil arranged in a grid pattern. The grid pattern maximizes the amount of metallic wire or foil subject to strain in the parallel direction. The cross sectional area of the grid is minimized to reduce the effect of shear strain and Poisson Strain. The grid is bonded to a thin backing, called the carrier, that is attached directly to the test specimen. The strain experienced by the test specimen is transferred directly to the strain gauge, which responds with a linear change in electrical resistance. Strain gauges are available commercially with nominal resistance values from 30 to 3000 Ω, with 120, 350, and 1000 Ω being the most common .

8

1.2.6. Piezoelectric Sensors

A Piezoelectric material may be defined as one that produces an electrical discharge when subjected to a mechanical deformation and undergoes a mechanical deformation when subjected to an electrical input. Polymeric materials that exhibit piezoelectric properties are suitable as a tactile sensors, polyvinylidene fluoride (PVDF) is a classical example of a polymer that is now widely being tested for use as tactile sensors. PVDF is available in sheets that are 5 microns to 2 mm thickness. It has good mechanical properties and can be molded to an appropriate shape with little difficulty. Metallization was used to apply a thin layer of metal on both sides of the PVDF sheet to collect the charge accumulated and to permit electrical connections.. As mentioned earlier, deformation caused by an external force results in an electrical charge that is a function of the applied force. This charge results in a voltage $V= Q/C$, where Q is the charge developed, and C is the capacitance of the device. Piezoelectric crystals act as transducers that turn force, or mechanical stress into electrical charge which in turn can be converted into a voltage. A Schematic of a piezoelectric sensor is shown in the figure 1-4.
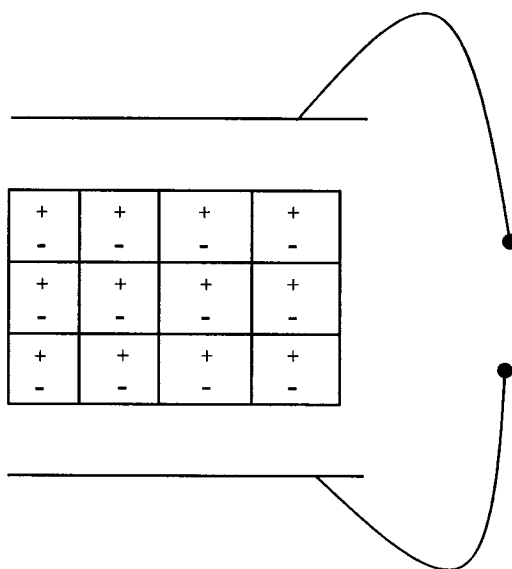
Figure 1-4. piezoelectric sensor

9

1.3 Literature Review

There has been many studies on the design and application of tactile sensors in robotics; however, despite its importance in medicine, comparatively limited research has been conducted in this area. One study that specifically looked at palpation quantified the main psychophysical parameters for lump detection in breast self-examination [11]. However they did not investigated mechanical issues such as finger motion and forces or induced pressure distributions on the fingerpad. Other studies have looked at the relation between tactile stimuli, mechanoreceptor response, and cognitive perception. Many of these, however generated tactile stimuli by pressing rigid objects against the fingerpad [12-14].

A capacitive micromachined endoscopic teeth-like pressure sensor capable of measuring a few grams of applied force was designed and fabricated [15,16].An array of micro tactile capacitive sensors developed for application of surgical endoscopes was found to exhibit severe hysteresis problems [17]. Dargahi et al. [18] have designed and fabricated a micromachined robust piezoelectric endoscopic tooth-like tactile sensor with a good linearity and a high dynamic range. However, this sensor is limited to measurement of dynamic loads only. Bicchi et al. [19] have measured the compliance and visco-elastic property of tissue using a sensitized laparoscopic device by measuring the grasper force and its angular displacement . Howe et al. [20] have reported a capacitive tactile sensor and an associated tactile display unit for use in minimally invasive surgery. An endoscopic sensor and actuator device was also attempted by Fisher et al. [21]. Many transducers such as compliant capacitive sensors [22,23] and optical sensors [24] have been proposed to measure distributed pressure. Howe [25] provides a

comprehensive review of performance specifications for tactile sensors, including spatial resolution, temporal response, range, accuracy, linearity, and hysteresis. Previous work on medical applications of tactile array sensors [26] was largely aimed at creating autonomous robotic palpation systems.

Recent studies have focused on the development and control of a microgripper based on flexure joints, fabricated by LIGA and instrumented with semiconductor straingauge force sensors [27]. Straingauge sensors located at the tip of the micro-gripper provide useful information for force control of the microgripper in biomedical applications. Majority of tactile sensor technologies have focused on silicon based sensors that use piezoresistive [28,29] or capacitive sensing [30,31] and polymer-based approaches that use piezoelectric polymer films [32,33] for sensing. A number of other techniques such as ultrasonic [34], pneumatic [35] and hybrid resistive [36] sensing have been explored to a lesser degree. Other works have combined some of the strengths of silicon with polymer-based devices, such as embedding silicon-sensing elements in polymer skins [37, 38], or covering silicon-based devices in a protective polymer layer [39]. Engel et al. [40] developed a polyimide-based two-dimensional tactile sensing array realized using a novel inverted fabrication technique. This is the first tactile sensor array based solely on polymer micromachining and thin-film metal resistors. The main advantages of this approach include increased robustness, decreased fabrication cost and complexity, low-temperature processing and improved strain transfer from membrane to strain gauges [41]. Shinoda et al. [42] have developed ultrasonic emission tactile sensor

11

that is capable of quick localization of touch and detouch, sensation of texture under movement and detection of precursor.

A novel acoustic tactile sensing system with an ability to identify the principal curvatures of the object surface by utilizing reflecting acoustic wavefronts has been proposed [43]. Dargahi et al., [44] developed a prototype of a tactile sensing system using three PVDF sensing elements. The magnitude and position of applied force on the sensor is obtained by using triangulation approach combined with membrane stress. Petter et al.[45] developed a new tactile measurement system, that is capable of differentiating the hardness of various soft materials like living tissues. In particular, it can detect harder inclusions within a softer matrix such as a timorous knot embedded within physiological tissue. The system measures the mechanical frequency response of the tissue. It is intended to integrate this "vibrotactile sensor" inside the top of a tactile rod for endoscopic surgery, in order to provide the surgeon a substitute for the missing tactile feeling. Locating arteries hidden beneath superficial tissue is a difficult task in MIS. Ryan et al. [46] developed a system, that can find the paths of arteries using tactile sensing in MIS. The surgeon begins by using the surgical robot to place the tactile sensor instrument on a known artery location. Signal processing algorithms locate the artery from its pulsatile pressure variation. The problems with compliance in the system result in occasional loss of the artery path. To perform MIS effectively, surgeons should be familiar with the Quantitative assessment of the biomedical properties of soft tissues. Many different layouts were proposed and designed for examining the tissue behavior while performing minimal invasive surgery. Yongping et al.[47] developed an ultrasound indentation system with a pen-size hand held probe, that is used to obtain the indentation

responses of lower limb soft tissues. A linear elastic indentation solution was used to extract the effective youngs modulus that ranged from 10.4 to 89.2 kPa for soft tissues. The Youngs modulus determined was demonstrated to be significantly dependent on site, posture, subject and gender. No significant correlation was established between the effective Youngs modulus and the thickness of entire soft tissue layers.

Dizaji et al. [48]   developed a new cancer diagnostic approach by ultrasonic imaging of tissues in which the tissue elasticity is measured and compared with the elasticity of normal tissues. The results of displacement estimation of normal and abnormal breast tissues under external stress are calculated using image registration technique. The work estimates not only the translation , but also the rotation and scaling parameters. The Youngs modulus calculated from displacement values was then used to identify tissue characterization. The work also showed that the above-mentioned procedure can successfully detect abnormal tissues. The latest developments in minimally invasive hapatic surgery was described by Guillaume et al.[49] , a new deformable model based on non-linear elasticity and the finite element method was proposed. This model is valid for large displacements, invariant with respect to rotations and therefore improves the realism of the deformations and solves the problems related to the shortcomings of linear elasticity, that is only valid for small displacements. problems associated with anisotropic behavior and volume variations were also addressed. Gladilin et al.[50] used a physical model based approach, where in a finite element based modeling scheme was implemented for static soft tissue prediction and muscle simulation. Scalari et al.[51] explained the problem of the in-vivo measurement of mechanical properties of soft

tissues, with particular emphasis on epidermis. The work also proposed a device based on pneumatic suction of tissues and preliminary results on human skin characterization, interpreted on the basis of an appropriate visco-elastic model were illustrated.

A non-invasive technique for quantitative determination of static mechanical properties of living tissue was proposed by Sumi et al [52]. In the proposed work, an inverse problem was hypothesized from which the spatial distribution of the relative elastic modulus of the tissue was estimated based on the deformation or strain measurement. The spatial distribution of the relative shear modulus was then obtained by spatial integration. This method seems promising for the quantitative differential diagnosis on the lesion in the tissue in vivo. .

In their work, Tritto et al. [53] used vascular fractal geometries to describe the coupling between elastic network deformation and vascular branching pattern modification under simulated controlled skin expansion. The work also tested the role of elastic organization of the skin, the interrelation between skin tension, line orientation, pedicle axis and the apparently random proliferation of the branching vascular pattern. Brouwer et al. [54] developed a device to measure the tissue properties under both in vivo and in vitro conditions. The former provides information about tissue behavior in its physiological state, while the latter provides better control over experimental conditions. The device developed was capable of measuring tissue properties under extension and indentation as well as recording instrument-tissue interaction forces.

Vacalebri et al. [55] designed and fabricated a miniature robotic system to perform in vivo mechanical characterization of soft tissue. The system employs a stepper motor controlled using microstepping techniques to prevent irregular rotation of motor shaft at lower rates, and a load cell to measure the reaction force of tissue under test. To minimize errors during evaluation of viscoelastic phenomena, a position and rate feedback control actuated by motor control using digital encoder was employed. Klaesener et al. [56] designed, built, and tested a portable indentor system that allows one to determine force/displacement measurements on soft tissue in a clinical or research setting. The indentor system consists of a load cell mounted on a three-dimensional measurement device (Metrecom), with the output of the load cell analyzed by software running on a notebook . The indentor device was tested on six different human soft tissues by two different investigators. The device was used to measure the soft tissue characteristics on the plantar surface of the foot of a subject which was than used to calculate the effective Youngs modulus of the tissue; The results indicate data from this device to be reliable, accurate and sensitive enough to identify mechanical properties of human tissues.

1.4 Comparison Of Different Technologies

Capacitive technologies coupled with semiconductor advancements holds great promise despite shielding problems. However, as with magnetostrictive devices, there still remains a lot more to be exploited.

The force-resistance characteristic of elastomer based sensors is highly nonlinear, requiring the use of signal processing algorithms. By the application of dynamic load, the

resistive medium within the elastomer migrates over a period of time .Additionally, the elastomer undergoes a permanent deformation and fatigue leading to permanent deformation of the sensor. This results in poor long-term stability of the sensor.

Magneto resistive devices have not developed well enough as to be compared with other technologies mentioned in this discussion.

Although Optical technology satisfies many of the requirements of an ideal tactile sensor such as high resolution, sensitivity and immunity to electromagnetic radiation, their application is severely limited by the brittleness of materials that go into building an optical sensor

Strain gauge sensor have low sensitivity, a very large time constant and a large drift associated with fatigue and hysteresis. Further more, they tend to be nonlinear and electrically noisy. Although some of these limitations are overcome by the introduction of carbon fibers that exhibit attractive features such as robustness and high electrical conductivity, they don't adequately fulfill the requirements of a competent tactile sensor.

Piezoelectric technology utilizing PVDF films possesses several advantages over other methods previously discussed. PVDF is light, rugged, inexpensive and is available in a variety of thicknesses ranging from 6 microns to 2mm. It is flexible enough to be formed to complex shapes and exhibits large pyroelectric and piezoelectric responses, making it attractive for the design of a highly sensitive tactile sensor. In addition to these, PVDF has a bandwidth ranging from near D.C to well into the Megahertz range. A lack of D.C response of PVDF is normally overcome by implementing a conductive

elastomer layer on the tactile sensing system. Piezoelectric polymers present an interesting avenue for the development of a tactile sensing system that can mimic the skin response of a human hand. . A detailed explanation of properties of piezoelectric polymer polyvinylidene fluoride (PVDF) is presented in Appendix-1.

1.5 Objective and Scope of Research

The main objective of this work is to design and fabricate a micromachined Piezoelectric Tactile Sensor that can measure both static and dynamic load simultaneously. A prototype was designed, fabricated and theoretical and experimental analyses were performed. The fabricated sensor was interfaced with electronics for signal amplification, capacitance and voltage measurements. The results were compared with 2D structural models and 3D modeling in ANSYS.

Tactile sensing and micromachining Technologies are discussed in the Chapter -2. Sensor design and fabrication is discussed in chapter-3 along with properties of materials used during fabrication. Chapter-4 deals with the analysis of the designed sensors using mathematical approaches and simulation using ANSYS. Experimental results and their comparison to theoretical analysis is described in chapter-5. Discussions of results obtained, conclusions and scope for future work are presented in chapter-6.

Appendix A presents a primer on piezoelectricity effect, properties and behavior of the PVDF films and analytical approach taken in designing the sensor using PVDF. Appendix B provides programs of simulation performed in ANSYS. Information on interfacing with electronics for signal amplification is described in Appendix C.

17

CHAPTER - 2

Silicon Micromachining Technologies

This Chapter describes the basic fabrication processes used to fabricate silicon sensors, as well as the mechanical characteristics of silicon.

2.1   Silicon Micromachining

Semiconductor sensors are transducers that convert mechanical signals into electrical signals that are widely used for the measurement and control of physical variables. Pressure sensors used in fluidic, pneumatic and tactile detection systems, accelerometers in navigational and air-bag deployment, magnetic sensors in position control, infrared and visible light sensors in air conditioning and automotive systems are some of the classical examples of semiconductor sensors at work. The list of applications of semiconductor devices is humongous and discussion of the same is out of scope of the following work. Over the past twenty years, interest in semiconductor sensors has been greatly fuelled by the application of microelectronic technology to the fabrication of mechanical devices. Micromachining technology takes advantage of the benefits of semiconductor technology to address the manufacturing and performance requirements of the sensor industry

Because sensors receptive to different physical variables are structurally different. In general, there is no single technology that can allow for fabrication of a wide variety of sensors. There are however two classifications in silicon micro-sensor technology

18

namely Bulk Micromachining and Surface Micromachining. Bulk-Micromachined sensors are made by accurate machining of a relatively thick substrate while Surface-Micromachined sensors are fabricated from stacked thin films. Both technologies however, use materials and processes borrowed from VLSI technology. The three processes of deposition, lithography, and etching are sufficient to construct a wide variety of mechanical structures required for specific sensors. Bulk micromachining was used for the fabrication of the tactile sensor presented in this thesis.

2.2 Mechanical Characteristics of silicon

Silicon is arguably the world's best-characterized material. It is very strong, being similar to steel in modulus of elasticity. Its lack of mechanical hysteresis makes it an almost perfect material for sensors, particularly when high performance is required. Silicon easily surpasses stainless steel in yield-strength and aluminum in strength to weight ratio. Although difficult to machine using traditional cutting tools, it can be chemically etched into various shapes. The mechanical properties of silicon are compared with other materials in Table 2.1.

The electronic properties of silicon are predictably sensitive to stress/strain, temperature, and other environmental factors, which means that silicon sensors can easily communicate with electronic circuitry for data processing. Taking advantage of its conventional role as an electronic material and an already advanced IC fabrication technology, Silicon can be exploited as a high precision, high strength and reliable mechanical material.

Materials	Yield strength 10^9 N/m^2	Young's modulus 10^{11} N/m^2	Density g/cm^3	Thermal Conductivity (W/cm^{0}C)	Thermal Expansion (10^{-6}/^{0}C)
Diamond	53	10.35	3.5	20	1
Silicon carbide	21	7	3.2	3.5	3.3
Iron	12.6	1.96	7.8	0.803	12
Silicon	7	1.9	2.3	1.57	2.33
Tungsten	4	4.1	19.3	1.78	4.5
Stainless steel	2.1	2	7.9	0.329	17.3
Aluminum	0.17	00.7	2.7	2.36	25

Table 2.1: Mechanical Properties of Materials.

Micromechanics become increasingly applicable wherever miniaturized mechanical devices and components must be integrated or interfaced with electronics. The continuing development of silicon in micro mechanical applications is only one aspect of the current technical drive toward miniaturization that is being pursued over a wide front in many diverse engineering disciplines. Silicon microelectronics continues to be the most obvious success in the ongoing pursuit of miniaturization. Four factors have played crucial role in this phenomenal success story:

1)   The active material, silicon is abundant, inexpensive, and can now be produced and processed controllably to unparalleled standards of purity and perfection.

2)   Silicon processing itself is based on very thin deposited films which are highly amenable to miniaturization.

3)   Definition and reproduction of the device shapes and patterns are performed using photo lithographic techniques that are also capable of high precision, and are amenable to miniaturization.

4)   Silicon microelectronic circuits can be batch fabricated.

2.3 Surface Micromachining

Surface micromachining is the fabrication of micromechanical structures by deposition and etching of thin structural and sacrificial films. Surface micromachining relies on encasing specific structural parts of a device in layers of a sacrificial material during the fabrication process. The sacrificial material is then dissolved in a chemical etchant that does not attack the structural parts. In surface micromachining, the substrate wafer is used primarily as a mechanical support on which multiple, alternating layers of structural and sacrificial material are deposited and patterned to realize micromechanical structures. Surface micromachining enables the fabrication of complex, multicomponent, integrated micromechanical structures that would be impossible with traditional bulk micromachining. Thus, simple microstructures like beams or membranes as well as complex structures like linkages or encapsulated resonators can be fabricated on top of a silicon substrate.

A typical surface micromachining process, shown in Figure 2-1 , begins with the deposition of a sacrificial layer, which is then patterned to create openings to the underlying substrate. Next, the structural layer is deposited and patterned into the desired geometry. Finally, the structural components are released by removal of the underlying and surrounding sacrificial material. The structural components are attached to the underlying substrate at the anchor region.

Deposition of
sacrificial layer

Patterning of
sacrificial layer

Deposition and
Patterning of the
structural layer

Sacrificial layer
etching

Free standing
micromachined
structure

Silicon
substrate

Silicon
dioxide

Poly-silicon
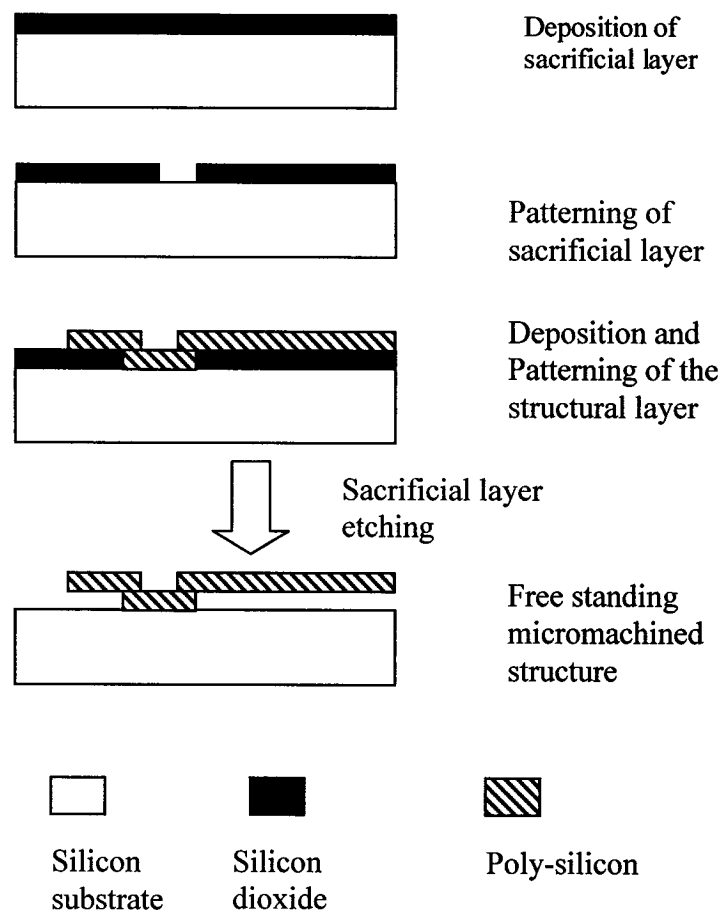
Figure 2-1. Crxcoss-sectional schematic demonstration of surface micromachining

22

2.4 Bulk Micromachining

Bulk micromachining is a subtractive process that involves the selective removal of the wafer substrate material to form the MEMS structure, which can include cantilevers, holes, grooves, and membranes. Bulk micromachining makes micromechanical devices by etching deeply into the silicon wafer. There are several ways to etch the silicon wafer. Anisotropic etching uses etchants like KOH that etch different crystallographic directions at different rates. Certain crystallographic planes etch extremely slowly, and are called stop planes. Anisotropic etching usually produces V- grooves, pyramids, and channels into the surface of the silicon wafer. Isotropic etching etches all directions in the silicon wafer with nearly the same rate, and produces rounded depressions on the surface of the wafer that usually resemble hemispheres and cylinders. When several bulk micromachined wafers are bonded together, a wide range of complex mechanical structures can be made.

There are a great variety of methods for bulk etching silicon. For a given application, the appropriate choice of etching method depends upon a number of factors, including the shape of the desired structures, the resulting surface roughness, etchant cost, equipment cost, safety, process compatibility, and availability. In cases that require etching simple structures like membranes, grooves, and reflective surfaces, beaker based wet chemical etching of silicon will be adequate. For other complex structural requirements like undercutting of delicate micrometer-scale mechanisms, dry-etching methods will be more appropriate.

2.5 Photolithography

Photolithography plays an important role in the fabrication of all micromechanical devices. During microelectronics device fabrication, there arises a need to selectively subject a portion of the sample to a variety of fabrication steps, leaving the rest of the sample untouched. Photolithography enables one to accomplish this. Photolithography is conducted in room illuminated yellow in color to reduce the adverse effects of light on the photosensitive resist material . In this process, photoresist (PR) is applied on a wafer that is spun on a chuck, The coated wafer is then dried in a owen, exposed to UV light and then developed using a developer. The purpose of the photoresist is to protect chosen regions of the wafer for subsequent fabrication steps. A schematic depicting of the process of photolithography is shown in the Figure 2-2.

Exposure

Positive resist
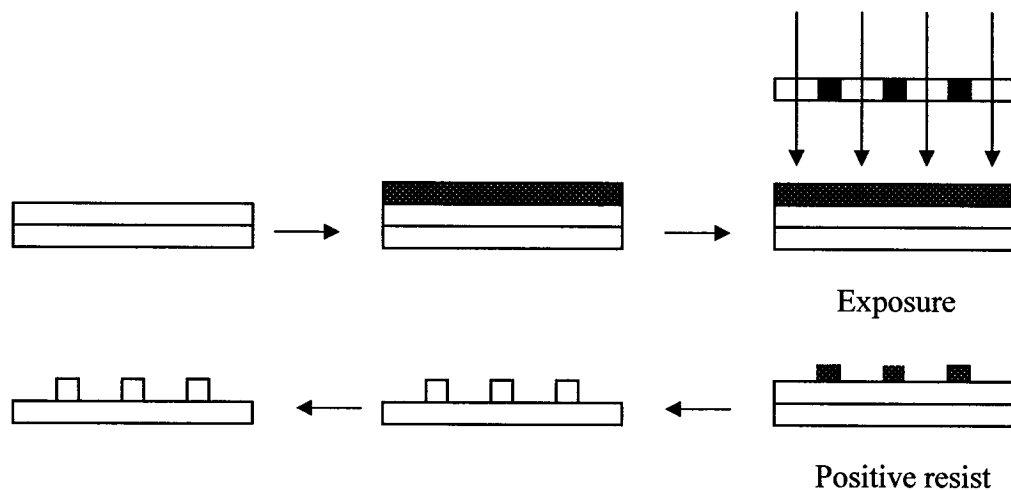
Figure 2-2. Photolithography process

The following chapter describes the design and the fabrication of tactile sensor, explained step by step.

24

CHAPTER - 3

Design of the Tactile Sensor

This chapter covers the process design and steps involved in fabricating the tactile sensor using standard photolithography and micromachining techniques.

3.1 Tactile Sensor

The tactile sensor consists of a silicon substrate with a PVDF film sandwiched between the silicon substrate and Plexiglass. Etching parameters were optimized to realize the cavity in the silicon substrate. The geometrical size of the sensor was selected from the design calculations performed. Two designs with different dimensions were realized. Both the designs had a silicon substrate as the base with 4 cavities and 20 μm as the cavity depth. The first design had a cavity length and breadth of 3mm while the second design had a length and breadth of 4mm and 2mm respectively. A patterned PVDF film of thickness 25 μm was placed above the silicon substrate in both the designs. A Plexiglass substrate was then structured to have a tooth-shaped profile, with a tooth thickness of 0.3 mm. Each tooth on the plexiglass substrate was separated by 1.1 mm. The schematic of the sensor can be seen in Figure 3-1 and The 3-D view of tactile sensor is shown in the Figure 3-2.
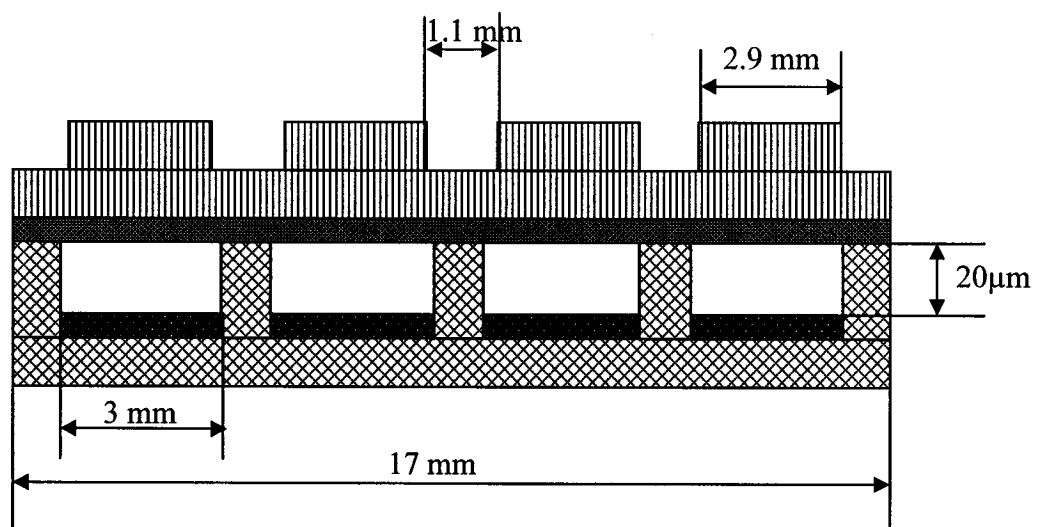
(a) Front- view
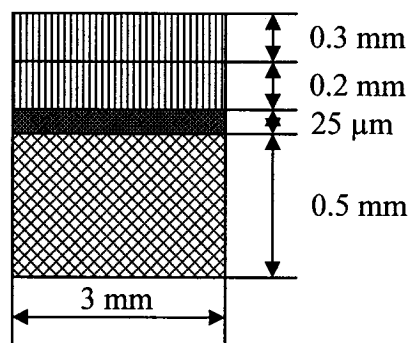
(b) side-view

Figure 3-1. Schematic of the Tactile Sensor
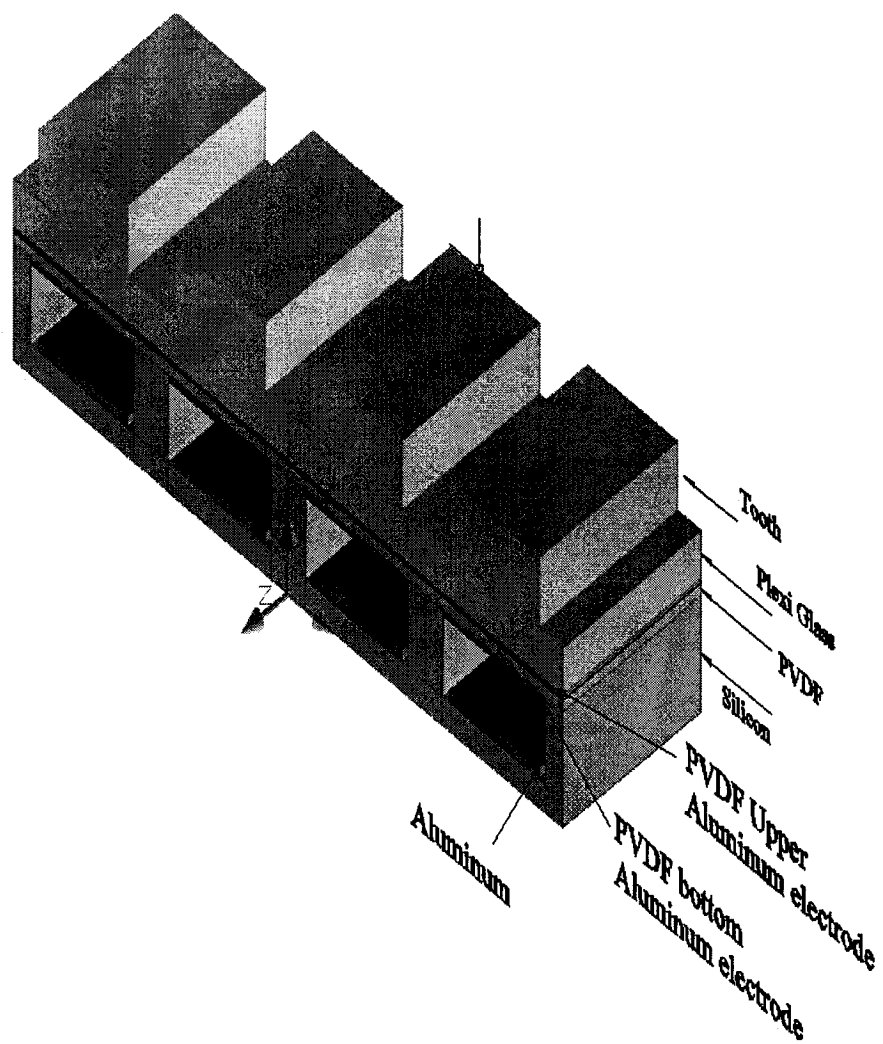
Figure 3-2. 3D view of the tactile sensor.

3.2 Materials Used for Fabrication of the Tactile Sensor

Silicon Substrate, PVDF , Plexiglass and Aluminum were the materials involved in the fabrication of the sensor. Since the mechanical properties of PVDF and plexiglass are very similar, the combination of these two was considered as a single beam. A <110> single side polished low p-doped silicon wafer of 0.5mm thickness was used in combination with a 25 μm PVDF film and 0.5 mm plexiglass substrate to complete the fabrication process. Aluminum was deposited in the cavities of the silicon substrate using an evaporator.

3.3 Process Design of the Tactile Sensor

As mentioned in section 3.1, the sensor structure comprises of three main parts namely silicon substrate, PVDF film and plexiglass substrate. Anisotropic etching of the Silicon substrate was done using TMAH to produce cavities on its surface. The bottom surface of each cavity was then coated with a layer of Aluminum using an evaporator. The bottom surface of an Aluminum coated PVDF film was patterned and the patterned surface was then aligned with the cavities in the Silicon substrate. Finally, a plexiglass substrate of thickness 0.5 mm was placed on the PVDF film and all three components were then glued together using a non-conducting glue capable of curing at room temperature in 5 minutes

The significant aspect of the sensor design is that, the fabrication procedure was carefully planned to satisfy the primary objectives of geometrical size and pressure range of the sensor. The tactile sensor requires 4 masking steps regardless of its geometric parameters. The mask design takes into consideration the size and tolerance required for

28

each masking step. The mask drawings required for processing the silicon wafers, selectively deposition Aluminum, patterning PVDF and plexiglass are presented in sections 3.4.

3.4 Mask Drawings for the Tactile Sensor

The mask drawing for the tactile sensor is presented in this section. Mask-1 is used to etch the cavities in the silicon wafer. Mask-2 is used for Aluminum electrode deposition in the cavities of the silicon wafer. Mask-3 and 4 are used for patterning the PVDF film and plexiglass. The "+" marks in all the four mask diagrams are the alignment marks used for assembling the sensor.
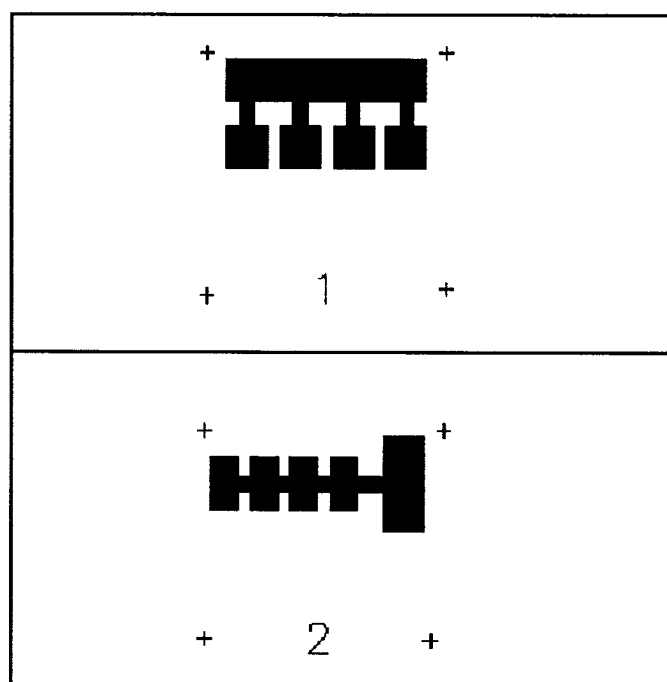
Figure 3-3. Mask-1: used to etch cavities in the Silicon wafer.

The mask design shown in Figure 3-3 is used to etch the cavities in the silicon wafer. The dark portions in Figure 3-3 represents the areas where the Silicon wafer is etched. Four alignment marks drawn on the mask are used for final assembly of the sensor. The shape and size of the cavity are different in the two designs. The cavity size in design-1 and design-2 are 3x3 mm and 4x2 mm respectively .
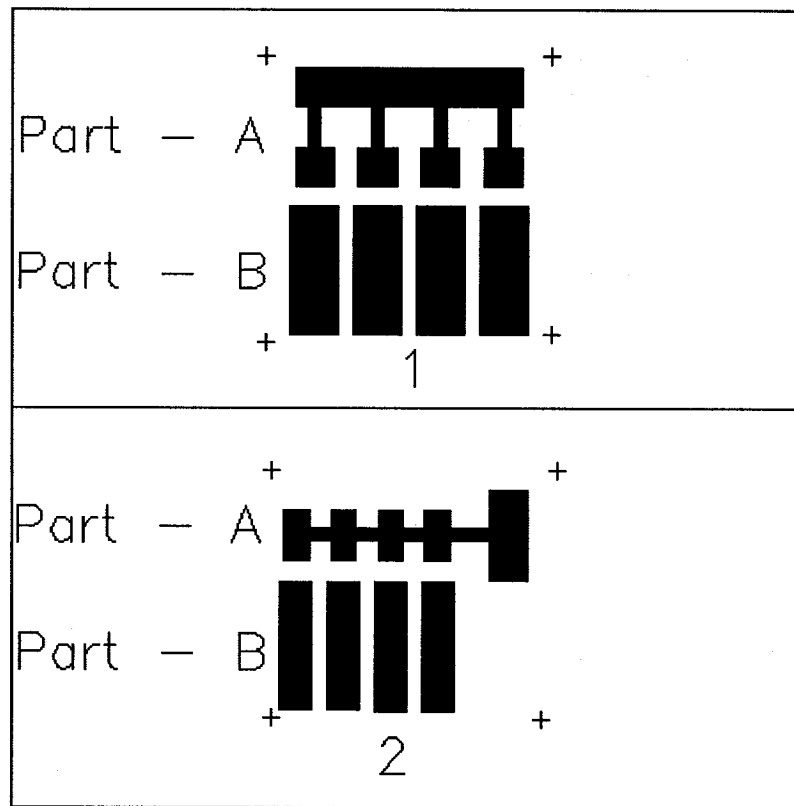
Figure 3-4. Mask-2: Used for Aluminum electrode deposition in the silicon substrate cavities.

The Mask design for selectively depositing Aluminum on silicon substrate is shown in Figure 3-4. The dark portions in the mask design represent the area on the Silicon wafer in which Aluminum is deposited. Alignment marks are used to make sure that electrodes are deposited in the desired position. Part A in Figures 3-3 and 3-4

represents the area in which Aluminum is deposited. Care was taken during the mask design in Figure 3-4 (by reducing its dimensions compared to the mask design in Figure 3-3) to ensure that Aluminum is deposited only on the floor of the cavity and not its walls. Part B in Figures 3-4 and 3-5 represents the area on the silicon substrate that is selectively deposited with Aluminum. This selectively deposited Aluminum acts as an electrode when brought into contact with the patterned bottom electrodes of the PVDF film.
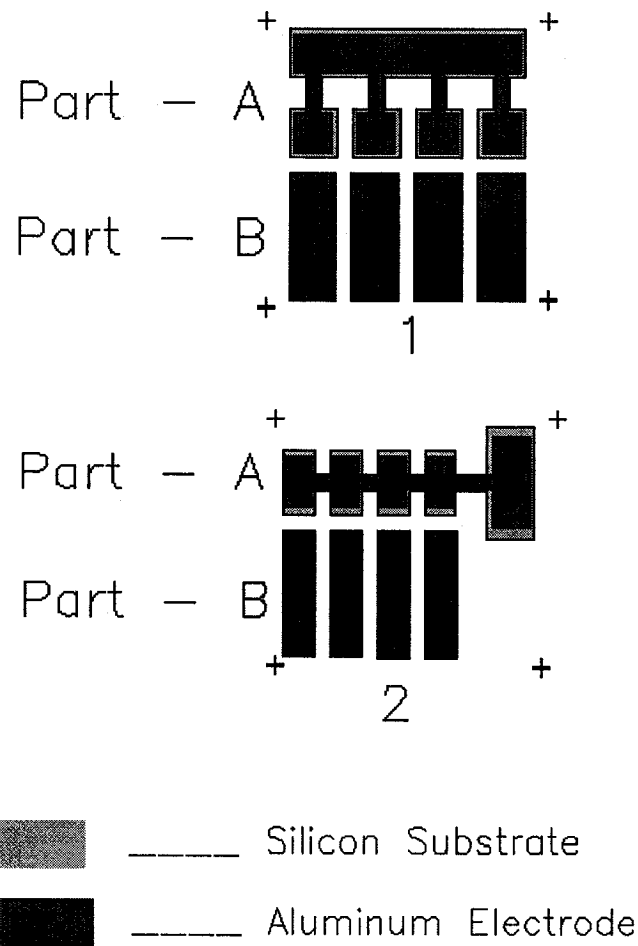
Figure 3-5. Top view of Aluminum selectively deposited on Silicon substrate

31
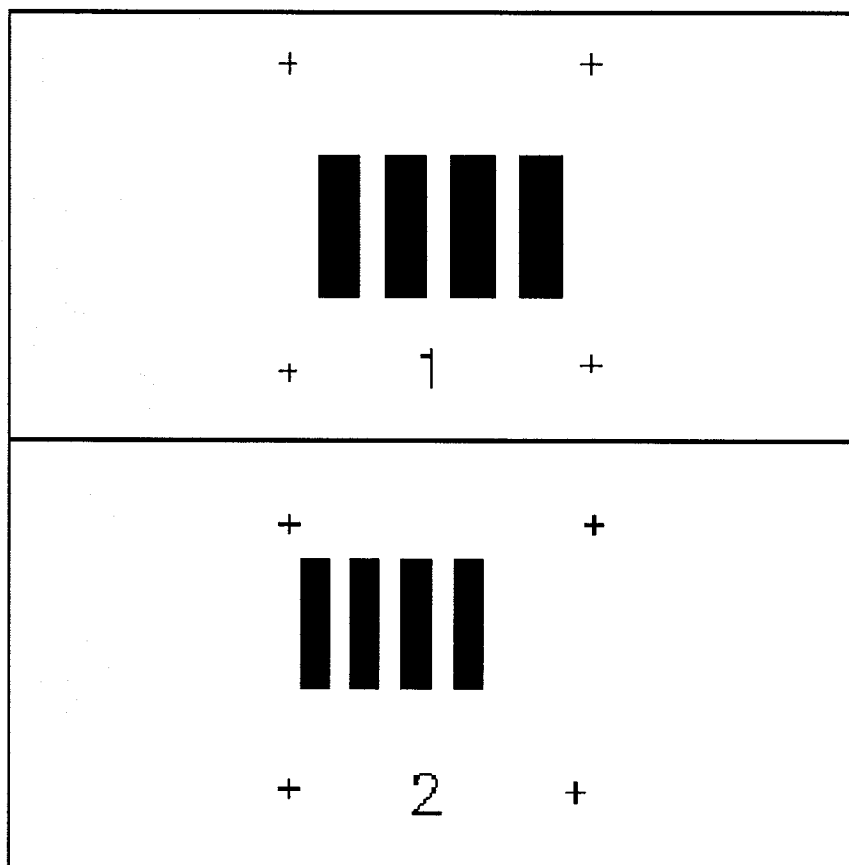
Figure 3-6. Mask-3: used for patterning the PVDF film

Figure 3-6 shows the mask design for patterning the aluminum electrodes on the bottom layer of the PVDF film. These electrodes are connected to the selectively deposited aluminum electrodes on the silicon substrate as shown in Figure 3-4 , Part-B.
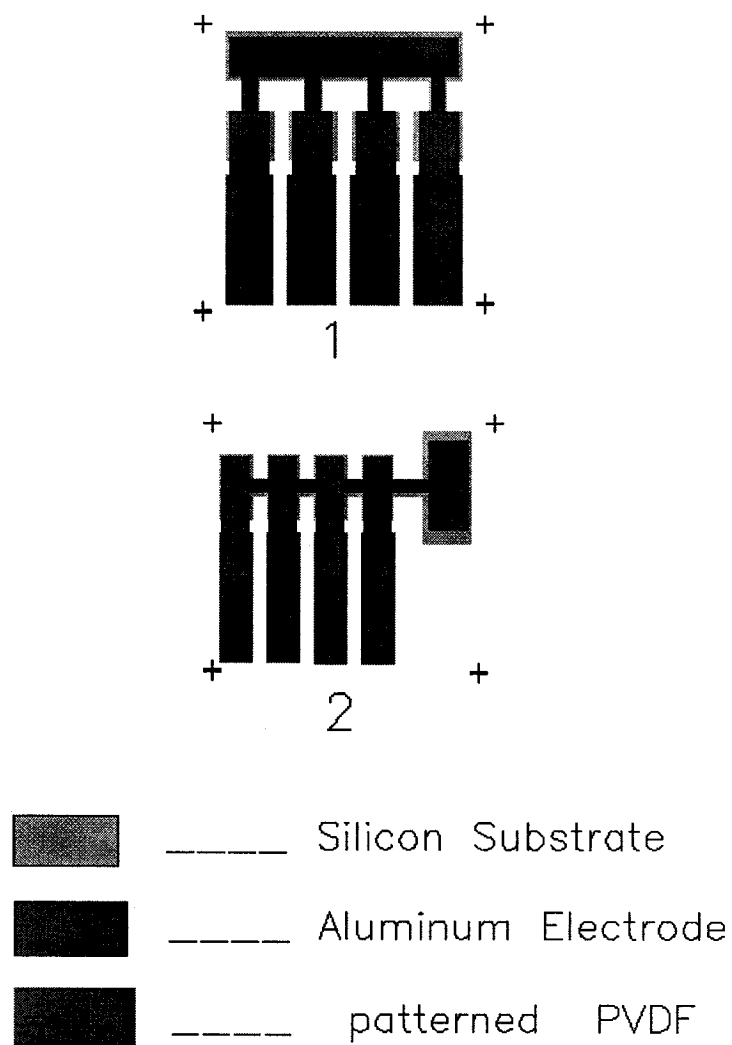
Figure 3-7. Top view of alignment of PVDF film with the silicon substrate.
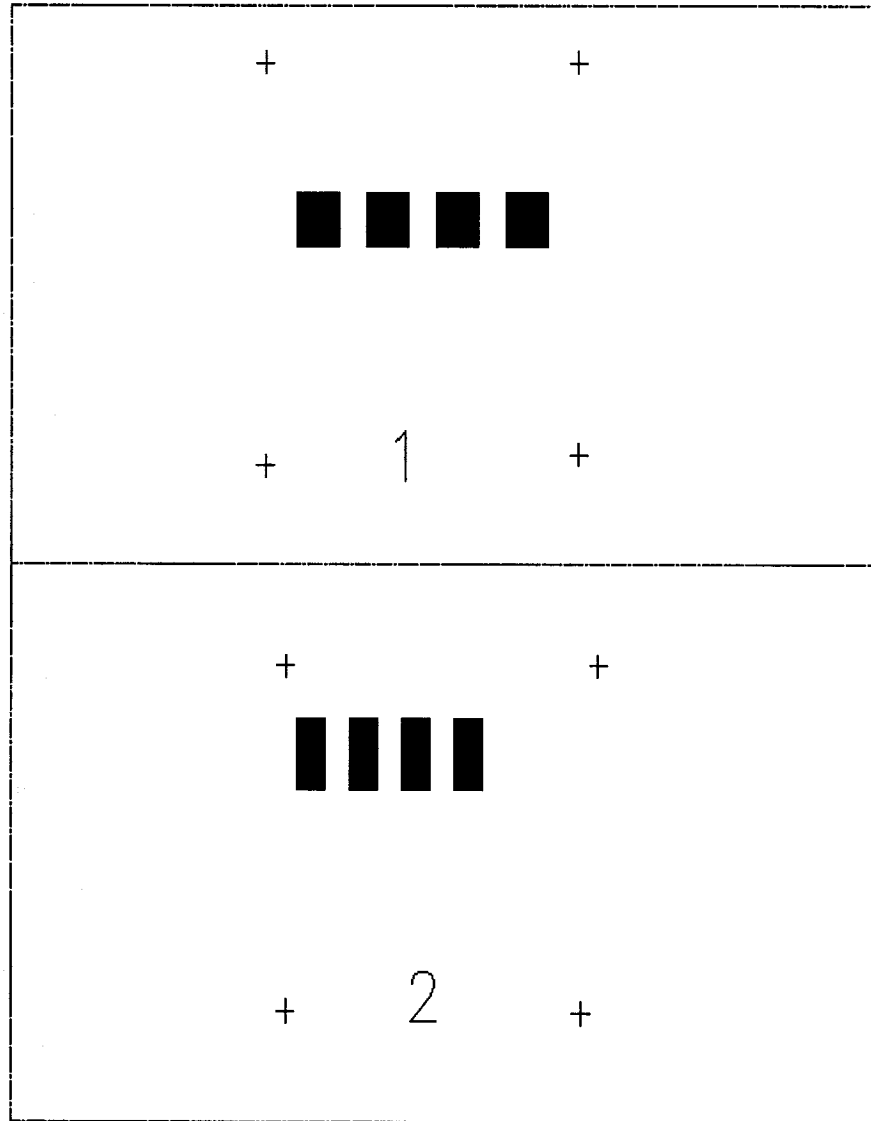
Figure 3-8. Mask-4: used to patterning Plexi-glass.

Figure 3-8 shows the mask design for etching tooth-shaped structures on the plexi-glass. The dark areas in Figure 3-8 show the teeth formed on the plexiglass and these teeth are aligned on top of the cavities in the Silicon substrate.
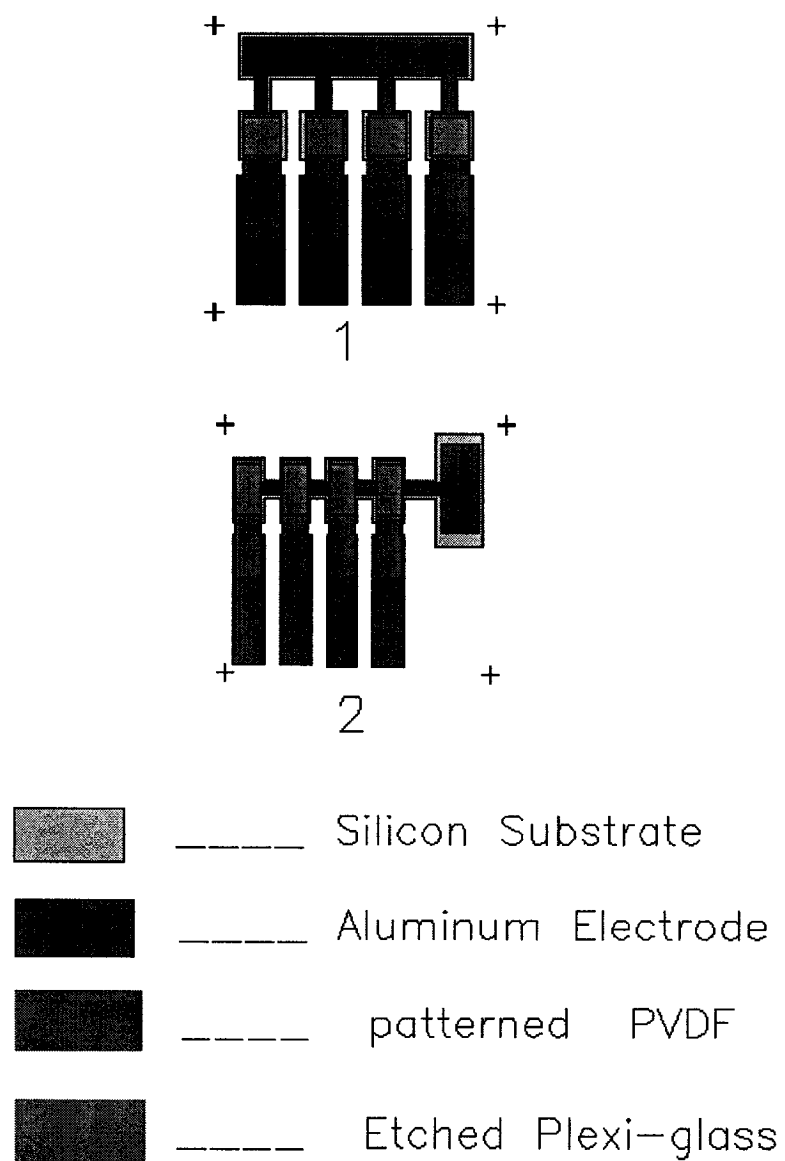
Figure 3-9. Top view of Alignment of Plexiglass with silicon substrate

35

3.5 Mask Making Using Photographic Techniques

3.5.1 Preparation of Glass Mask

The mask patterns shown in Figure 3-3 to Figure 3-9 were made using a drafting software (Auto CAD). And than transferred on to transparency sheets using a printer. The dimensions of patterns on the transparent sheets are the same as the actual design. The patterns were transferred (on to photo-sensitive glass masks) by bringing them into contact with the masks and by exposing the assembly to white light (at 500 Watts) placed at a distance of 30 cm for 1 second.

3.5.2 Preparation of Developer

To develop the photosensitive glass, D5 developer mixed with DI water in a 1:4 proportion was used.

3.5.3 Preparation of Fixer

F-4 fixer mixed with DI water (1:4) was used to fix the developed photosensitive glass.

3.5.4 Process Technology for Mask Making

The transparency with the mask drawing was placed on top of the photosensitive glass and exposed to a 500 Watt white light. The exposure time and distance between the light source and the photosensitive glass was empirically determined to be 1 sec and 30 cm respectively. The exposed mask was then developed at room temperature in the

developer solution with gentle agitation for 1 to 2 minutes until there was a clear image on the mask (photosensitive glass). In the next step, the mask was rinsed with filtered DI water. The mask was then placed in the fixer solution at room temperature for 1 minute and rinsed with DI water. Finally, the mask was dried and stored in a clean container stored in the clean room. The procedure described was repeated to prepare all masks for the tactile sensor.

3.6 Fabrication Process of the Tactile Sensor

The fabrication process of the tactile sensor chip is divided into 4 main streams, each corresponding to a layer of the sensor. The device was constructed as a sandwich structure with plexiglass, and the PVDF film bonded to the silicon wafer with the help of non- Conducting glue. The details of the each stream of fabrication is described below.

Figure 3-10 describes the sequence of operations carried out to realize the desired tactile sensor.

cleaned
silicon wafer
(section 3.6.1)

oxide layer
deposition
(section 3.6.2)
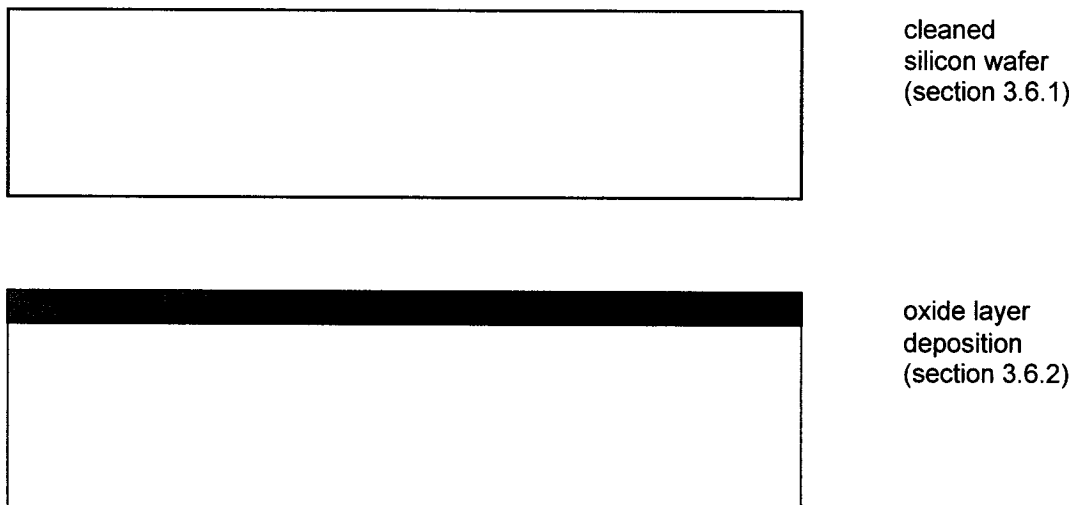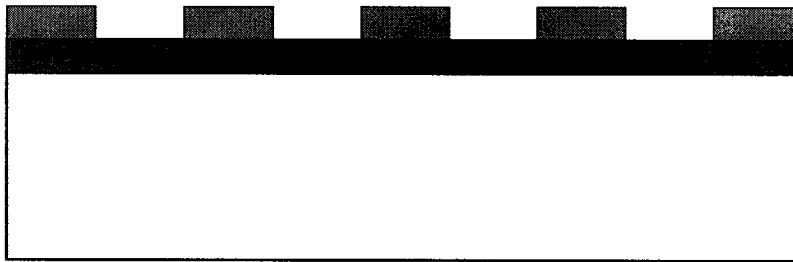
photolithography
used to open the
windows
(section 3.6.3)
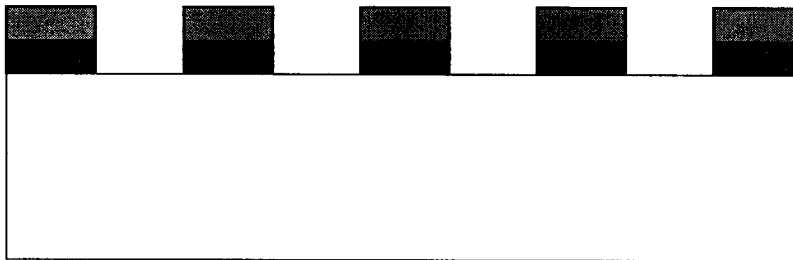
silicon dioxide
etching
(section 3.6.4)
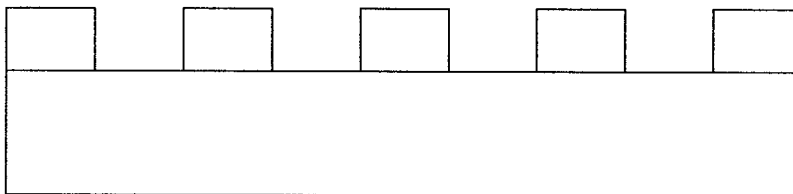
silicon etching
(section 3.6.5)
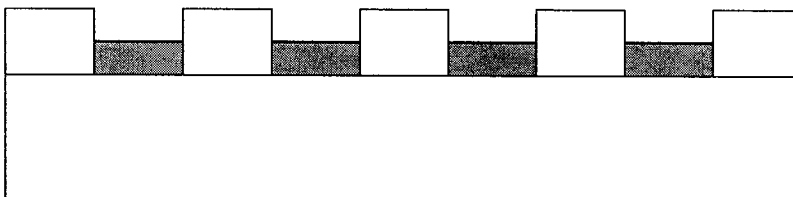
Aluminum
deposition
(section 3.6.6)

PVDF film with
aluminum on
bothsides

patterning of
PVDF
film
(section 3.6.7)

38

patterning of
plexiglass
(section 3.6.8)

Aligning of
PVDF and
plexiglass
(section 3.6.9)

Assembling of
tactile sensor
(section 3.7)
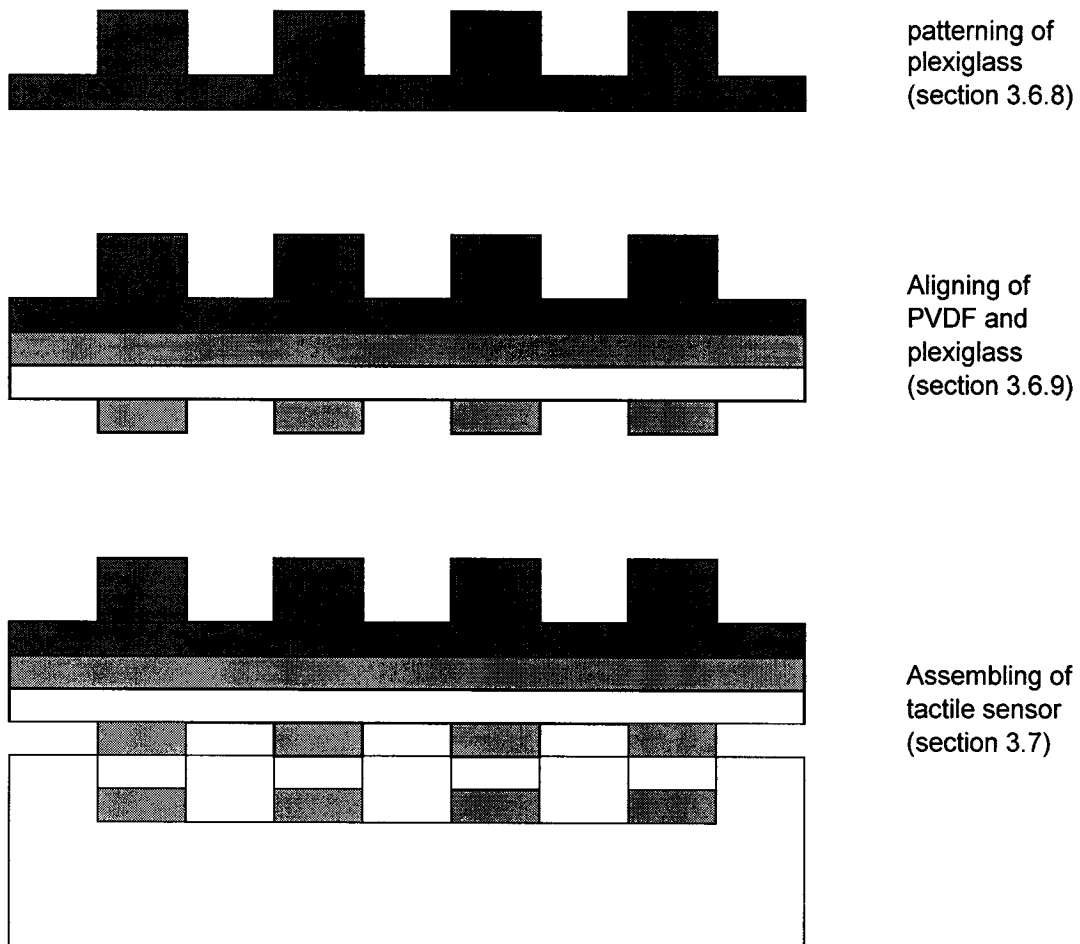
Figure 3-10. Fabrication sequence for tactile sensor

3.6.1 Silicon Wafer Cleaning Process

The silicon wafer was cleaned to eliminate unwanted impurities like dust, sodium, aluminum and native oxide. The cleaning process carried out is described as follows:

- The Silicon wafer was placed in a solution of H_2SO_4 and H_2O_2 mixed in a 1:1 ratio (80ml:80ml) and heated for 5 minutes and then rinsed with DI water.

39

- The wafer was then immersed in a solution of HCl, H_2O_2 and H_2O mixed in a 1:1:5 ratio (25ml:25ml:125ml) and then rinsed in DI water.

- Finally, the wafer was immersed in a solution of HF and H_2O mixed in a 1:50 ratio (2ml:100ml) for about 30 -60 seconds and rinsed with DI water.

3.6.2 Thermal Oxidation of Silicon

Thermal Oxidation, the process of growing an oxide layer on the surface of the Silicon wafer was done using the setup shown in Figure 3-11. Wet Oxygen was passed through a saturator filled with DI water maintained at temperatures between 96 °C and 100°C, well below the boiling point of water to avoid undue depletion of water molecules on the surface of the wafer. The equation representing the oxidation process is shown below:

$$Si + 2H_2O \rightarrow SiO_2 + 2H_2$$
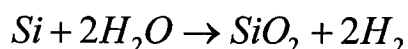
The samples (batch of Si wafers) were loaded in a Quartz boat. The boat was placed at the mouth of the oxidation chamber for 5 minutes before being moved to the center of the chamber. At the end of the prescribed time for oxidation, the wafers were allowed to cool for an hour inside the chamber and then stored in DI water to prevent atmospheric contamination until further processing.

Wrap –
Around

Resistance
Heated

The
Samples

Wet O_2

Quartz
Reacto

Resistance
Heated

Quartz Boat

Condensati
on Trap
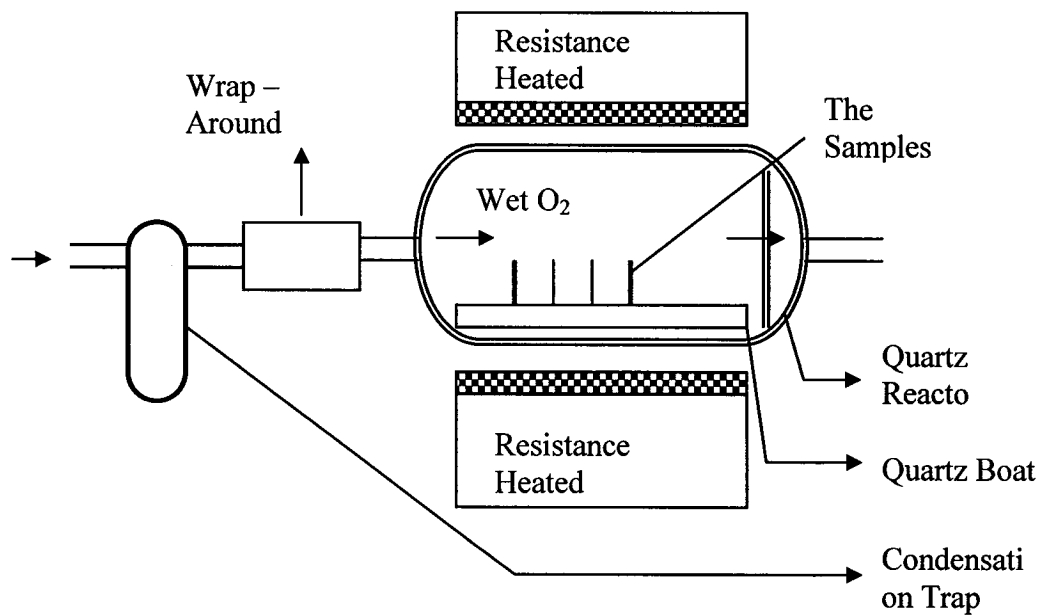
Figure 3-11. Schematic of Oxidation furnace Set up

3.6.3 The Photolithography Procedure

- The sample (Si wafer) was centered and secured on the spinner chuck using vacuum. Dust particles on the wafer were blown off using purified compressed Nitrogen. Three drops of negative photoresist (HNR-120 Resist-OCG-microelectronics materials Inc) was applied on the wafer which was then spun at 3000 rpm for 30 seconds.

- The wafer was soft baked in a forced air convection oven at 95^0C for 30 min. it was than allowed to cool at ambient temperature for 15 min.

- The wafer was placed on the mask aligning instrument and aligned using the X-Y table. The wafer was then exposed to UV-light for 10 sec from beneath.

- After exposure, the wafer was developed for 45 seconds and rinsed with DI water. It was then dried with purified N_2 at 20 psi.

- The wafer was hard baked in a forced convection own at 115°C for 30 minutes to get it ready for the next processing step.

41

3.6.4 Silicon dioxide Etching

- The wafer was dipped in a 1:4 (25-ml: 100-ml) solution of HF: N H_4F in a Teflon beaker for 2 min.

- The wafer was dipped in a 1:50 (3-ml: 150-ml) solution of HF: H_2O in a Teflon beaker and checked for hydrophobic surface at the window opening on the wafer. The process was repeated until a hydrophobic surface was observed.

- The etched wafers were then cleaned with DI water.

- Photoresist on the wafer was removed by dipping it in acetone.

3.6.5 TMAH Etching of Silicon Substrate

A constant temperature beaker- in- beaker apparatus was used for etching silicon in TMAH solution. A schematic drawing of the etching apparatus is illustrated in Figure 3.10. The apparatus consists of two beakers: a 250 ml Pyrex beaker placed inside a 1000 ml Pyrex beaker. The inner beaker was held on a plexi-glass support mesh placed in the larger beaker. The two beakers were placed in an enclosed electric heater. The inner beaker was maintained at a constant temperature of 90°C by heating the oil in the large beaker.

A Teflon multiple wafer holder was used to hold the wafer in a fixed position inside the etchant. This Figure 3-12 illustrates the wafer holder wherein the wafers are placed inside rows of cavities provided .
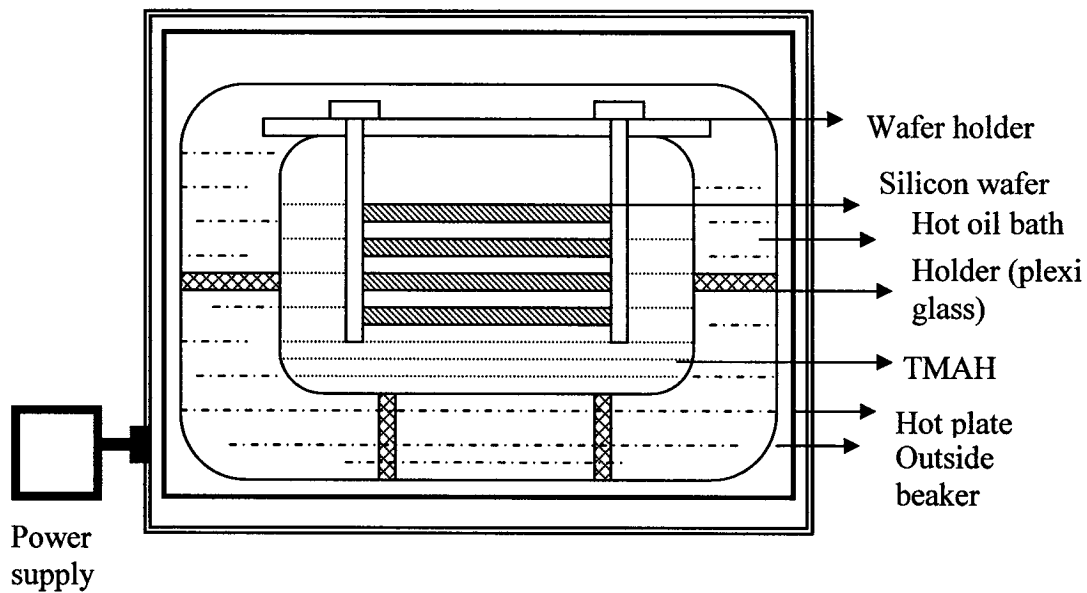
Figure 3-12. Silicon etching setup

3.6.6 Aluminium Deposition on Silicon Substrate

Aluminum was deposited on the silicon substrate using "Metal" Evaporator. The following procedure was implemented :

- Photoresist was again applied on the wafer and patterning via photolithography was done to reveal only the area in which Aluminum is selectively retained.

- Evaporator requires 45 minutes of warm up with a continuous water supply throughout the operation.

- Sample was loaded carefully by removing the top cover and cleaning the loading chamber with mild acid and sticking the sample in the chamber with the help of a sticking tape.

- Aluminum strings were loaded into the cleaned filament coil.

- The Aluminum strings were heated to their boiling temperature while the chamber was maintained at high vacuum. Aluminum was deposited on the

43

wafer. A thickness monitor was employed to monitor the thickness of deposition. A 30 second period yielded a thickness of 30 A°.

- Selective deposition of Aluminum is realized by dipping the wafer in Acetone to remove Aluminum in unwanted areas.

An image of the etched Silicon wafer with Aluminum deposited in the cavities is shown in Figure 3-13.

Aluminum deposited

Selective Aluminum deposition on the
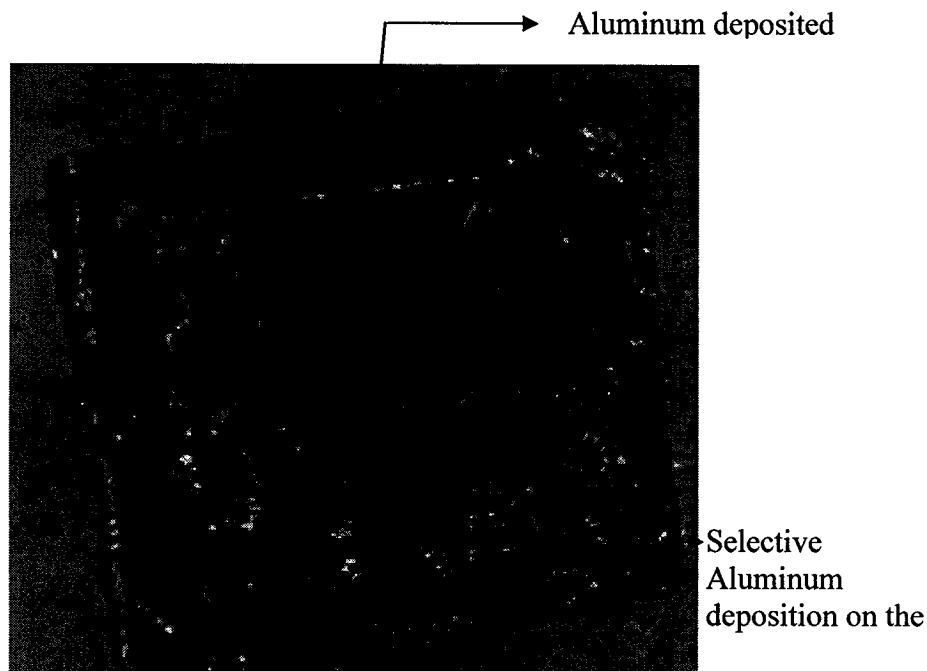
Figure 3-13. Image of Etched Silicon Wafer with Aluminum Deposition

3.6.7 Patterning of the PVDF Film

Aluminum was patterned onto the surface of the PVDF using photolithographic techniques. First, The PVDF film was glued on a bare Silicon wafer with a positive photoresist. The wafer with PVDF glued on it was held in a vacuum chuck, and 15 ml of photoresist was dispensed at the center. The wafer was than spun at 4000 rpm for 30 sec. This results in an even layer of photoresist, that was dried and semi-cured by soft baking

44

at 60°C for 40 min. A mask with the desired pattern was used to transfer the desired electrode pattern onto the PVDF film by exposing it to UV light The exposed wafer was developed or 45 seconds, rinsed in DI water, air dried and then cured in a hard bake oven at 60°C for 40 minutes. Commercial Aluminum etchant, a mixture of phosphoric acid : Acetic acid : Nitric acid : water (73 % : 11.5% : 2.5% : 13%) was used to etch aluminum . The wafer was dipped in the etchant solution for about 1 hour until the aluminum was etched in the required area. Acetone was later used to remove the PVDF film from the Silicon wafer . After repeated trials, it was noticed (Figure 3-14(a)) that it was not possible to protect the aluminum electrode beneath the PVDF film attached to the Silicon wafer. So, an alternate method (Figure 3-14 (b)) was tried wherein the PVDF film was patterned by applying the etchant directly on it using a brush while constantly monitoring the area etched using a magnifying glass.

Patterned bottom electrodes of PVDF

Figure 3-14. (a)

Image of Patterned bottom electrodes of PVDF obtained after photolithography

(b)
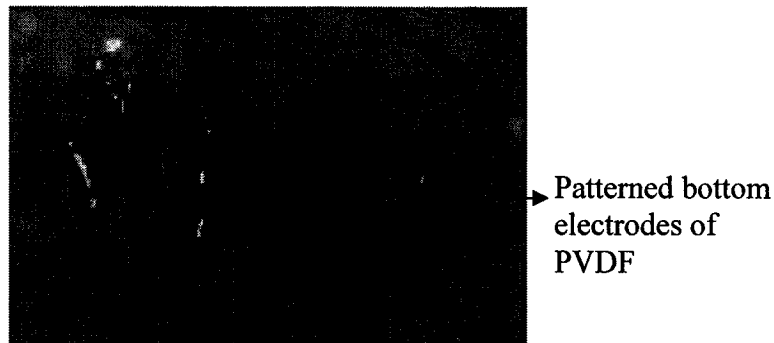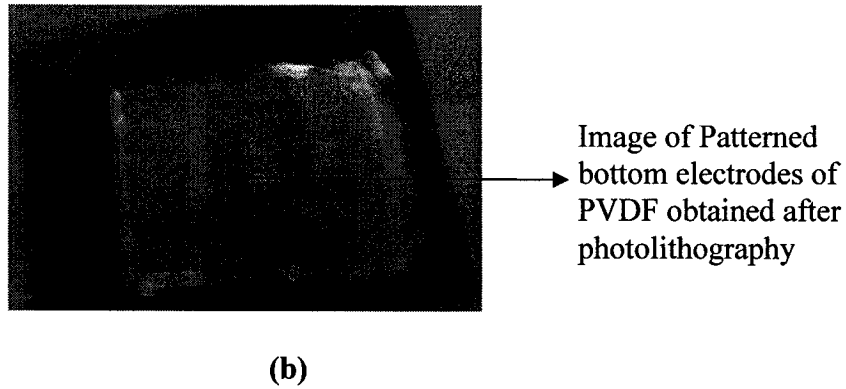
Figure 3-14. a) Unanticipated removal of Aluminum electrode from underside of

PVDF film. b) Alternate method for electrode patterning on PVDF film.

3.6.8 Patterning of Plexiglass

The teeth of the tactile sensor were patterned onto the surface of the plexiglass using the mechanical technique of filing. First, alignment marks were drawn on the plexiglass in such a way that the filed teeth would be positioned exactly above the etched cavities in the Silicon wafer cavity. As mentioned earlier, teeth on the plexiglass were filed carefully under a magnifying glass. Care was taken to ensure that the space gap between each tooth was the same as the space between each etched cavity in the Silicon wafer. The plexiglass used had a thickness of 0.5 mm and the gap between each teeth.

3.6.9 Aligning of PVDF and Plexiglass

For proper functioning of the sensor, the teeth of plexiglass should be aligned exactly above the patterned lower electrodes of the PVDF film. Misalignment would result in a non-uniform displacement of the film and consequently an error in both capacitance and voltage change. In order to have proper alignment, the plexiglass and PVDF film were cut in exact size and glued together under the magnifying glass.

46

3.7 Assembling The Tactile Sensor

The silicon wafer and PVDF film with plexiglass on the top of it were bonded together by using non conducting glue. The silicon substrate was placed on a flat glass plate very carefully and the plexiglass with PVDF under it was glued to the silicon substrate in such a way that the cavities on the silicon substrate were properly aligned with the electrodes and teeth of the PVDF film and plexiglass respectively . Extreme care was taken not to put an excessive amount of the glue that might run into the cavities in the silicon substrate. After drying the assembly in ambient for a few minutes, The bond was found to be strong and durable.

In the next chapter, modeling of the tactile sensor is explained using analytical and numerical (ANSYS) calculations of the deflection of the membrane followed by a comparison of both models presented.

CHAPTER - 4

Modeling of the Tactile Sensor

4.1 Analytical Model

The tactile sensor design was modeled both analytically and in ANSYS for the following reasons:

- To predict the functionality of the sensor.

- To understand and estimate the sensitivity of the device.

4.2 Assumptions

In order to develop a simple analytical model for deflection analysis, the following assumptions were made:

- The structure of each tooth is a simple beam with two fixed supports as illustrated in Figure 4-1.

- The material properties and loading conditions are assumed to be uniform.

x Point of deflection

W

$\delta(x)$ $\delta(max)$

L
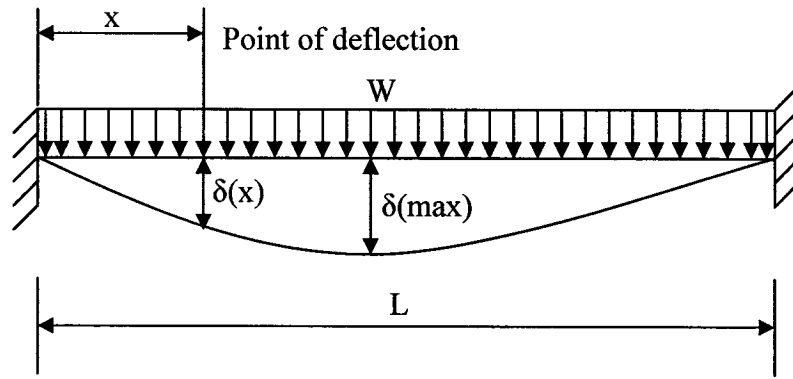
Figure 4-1. Representation of a basic theoretical approach for modeling an endoscopic tactile sensor.

Based on the above model, an applied pressure of W at the tip of the tool will

produce a deflection of δ, which is given by [57]

$$\delta(x) = \frac{WL^4}{24EI}\frac{x^2}{L^2}\left(1-\frac{x}{L}\right)^2 \qquad (4.1)$$

The maximum deflection of the fixed beam shown above occurs at the center of the beam which is at x = L/2.

$$\delta(max) = \frac{WL^4}{384EI} \qquad (4.2)$$

Where   W = Applied pressure
L = Length of the tooth
x = point of deflection
E = Youngs modulus
I = Moment of Inertia

49

4.3 Calculation and Results of the Analytical Model

Figure 4.2 shows a plot of deflection of the membrane with an pressure of 0.133 N/mm^2 is applied It can be seen from the figure that the maximum deflection occurs at the center. The deflection is represented in μm.
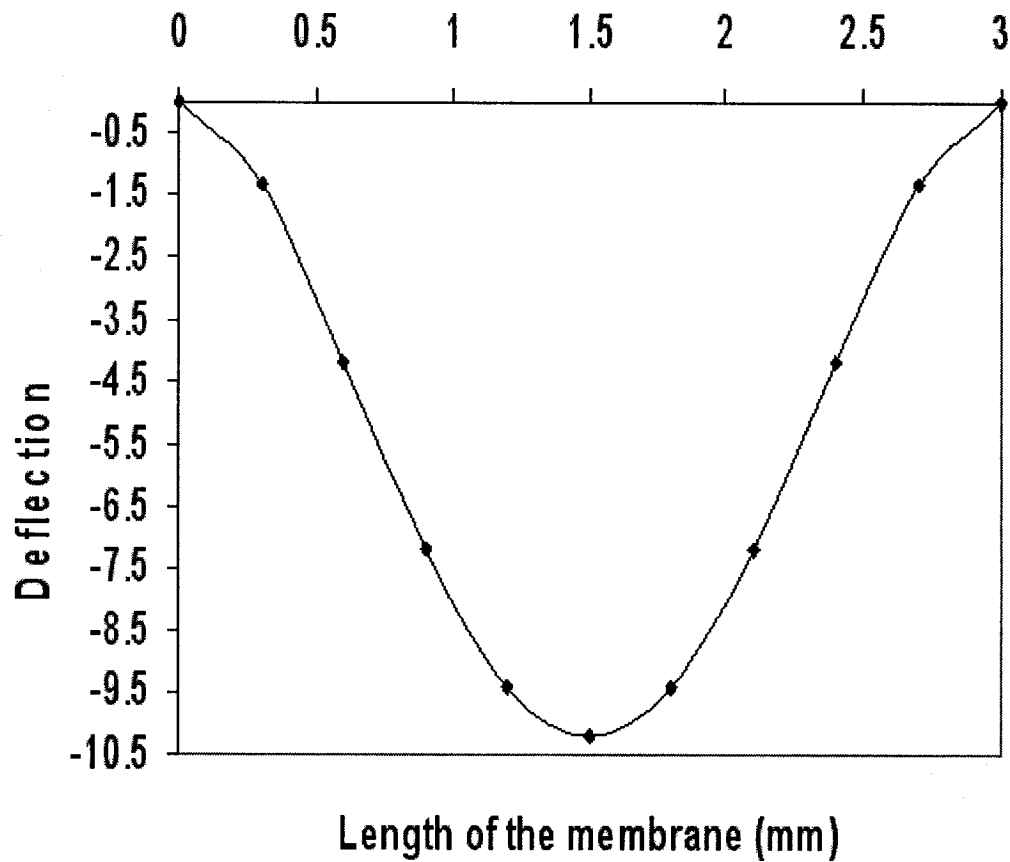
Figure 4-2. Analytical model plot of deflection across the membrane.

4.4 Capacitance Calculations

The Capacitance between two plates is given by:

$$C = \varepsilon_r * \varepsilon_o * \frac{A}{d} \qquad (4.3)$$

Where ε is the permittivity of the medium, A is the area of the electrodes and d is the distance between the electrodes. In the present case, the change in capacitance is

$$C = \varepsilon_r * \varepsilon_o * A \int_0^l \frac{1}{d^1 - \delta(x)} dx \qquad (4.4)$$

Were d^1 is the depth of the cavity and $\delta(x)$ is the deflection curve of the membrane obtained from equation (4.1).
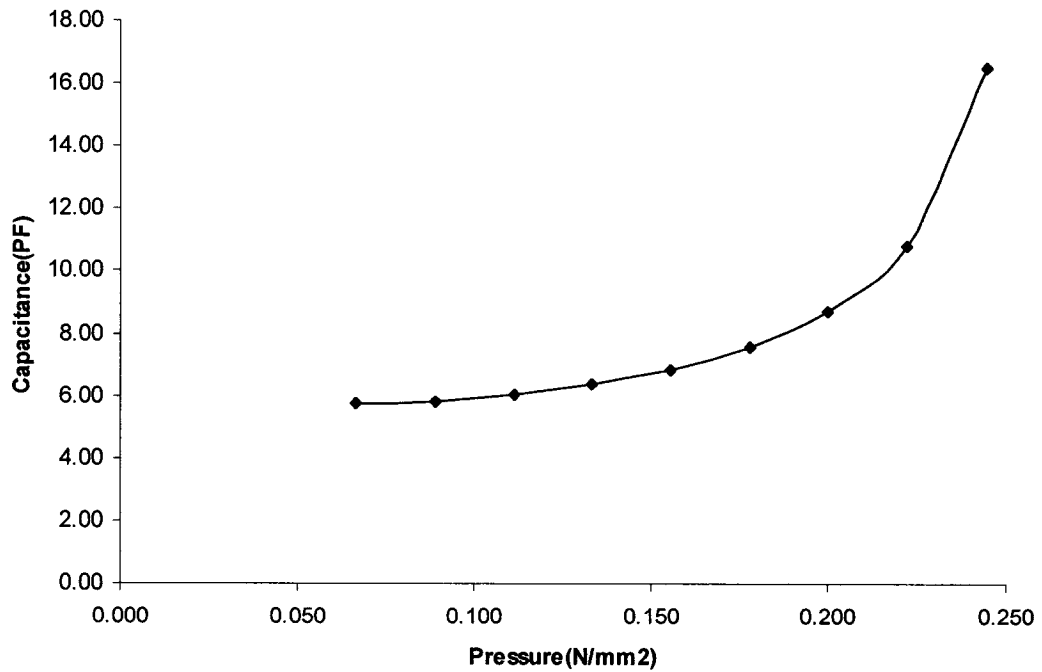
Figure 4-3. Plot of pressure versus capacitance.

51

Figure 4-3 shows the plot of pressure versus capacitance output. It can be seen from the plot that capacitance between the bottom electrode of PVDF film and aluminum electrode on the cavity increases with the increasing load.

4.5 Finite Element Model

Finite element modeling is a numerical method of solving engineering and mathematical physics problems in the areas of structural analysis, heat transfer, fluid flow, mass transport, involving complicated geometries, loadings, and material properties.

This research employs the commercial finite element analysis package ANSYS (version 6.0). The software was used to construct an element model of the tactile sensor that was used to predict the deflection of the PVDF membrane under an applied pressure on the tooth of the sensor.

To use the program, a finite element model of the designed micromachined tactile sensor is defined and information regarding the position of the element nodal coordinates, the manner in which the elements are connected, the material properties of the elements, the applied load and boundary conditions, and the kind of analysis to be performed is fed into the program. This is the very first step of the procedure and is called preprocessing. In the second step, solving, the program uses the information from the preprocessing step to generate and solve the equations to carry out the analysis. In the final step, postprocessing, the raw solution data generated after solving step can be translated to color graphs and contours for easy interpretation and viewing of results.

4.5.1 Nodal Analysis

A detailed listing of all the inputs and outputs for the nodal analysis is explained step by step. After entering the ANSYS program, the preprocessor was entered to define the model. From within the preprocessor, the structural analysis type was selected. An element type of "solid 45", a three dimensional structural brick with 8 nodes at the corners was selected. The next step is defining the material properties youngs modulus and density for all the three different materials used in the design namely silicon, PVDF and Plexiglass. For simplicity, the basic units Newton and millimeters were used. A three dimensional solid model of the single teeth of the tactile sensor is defined graphically. Figure 4-4 shows the model of the single tooth of the grasper.

Boundary conditions applied approximated the model to the clamping of the membrane on top of the Silicon substrate. Boundary conditions were applied by isolating the nodes along the edges and by constraining all their (edges') degrees of freedom using the displacement command under loads.

A uniform pressure was applied on the tooth and the deflection of the membrane was determined. Figure 4-5 shows the shape of the model after the pressure was applied. The maximum deflection at the center of the membrane can be noticed by the color coding used in the figure. Elements and nodes were generated over the solid model after it was volume meshed.

Figure 4-4. ANSYS Model of single tooth of the grasper
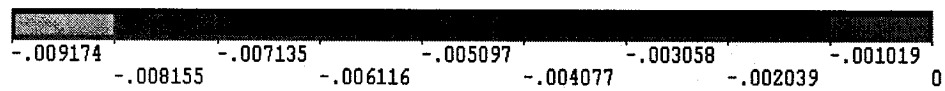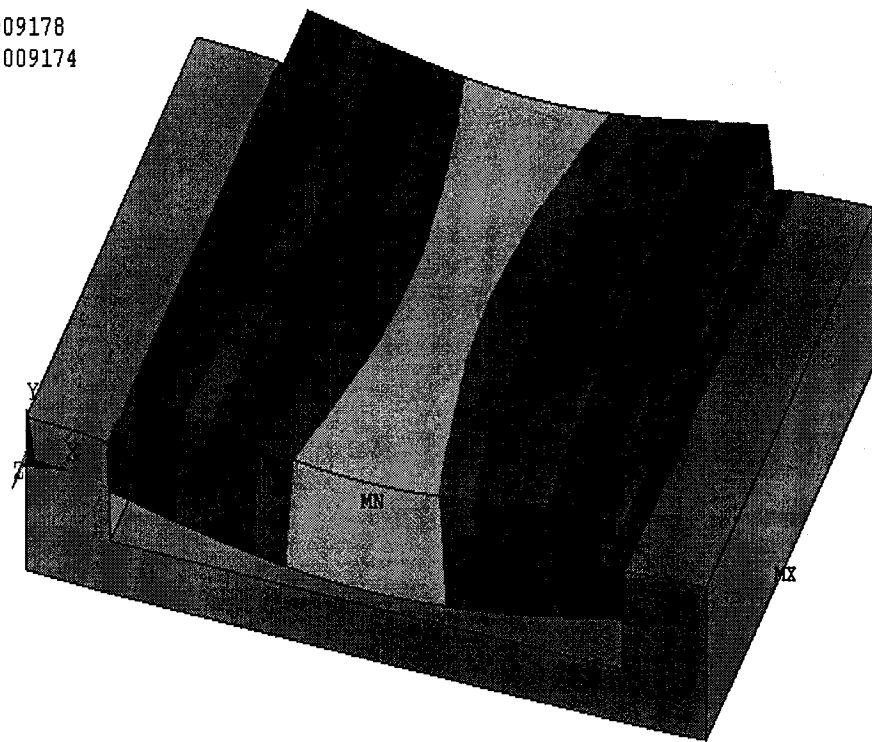
Figure 4-5. ANSYS model of a tooth of the grasper under pressure.

As it can be seen the maximum deflection obtained above is 9.174 μm.
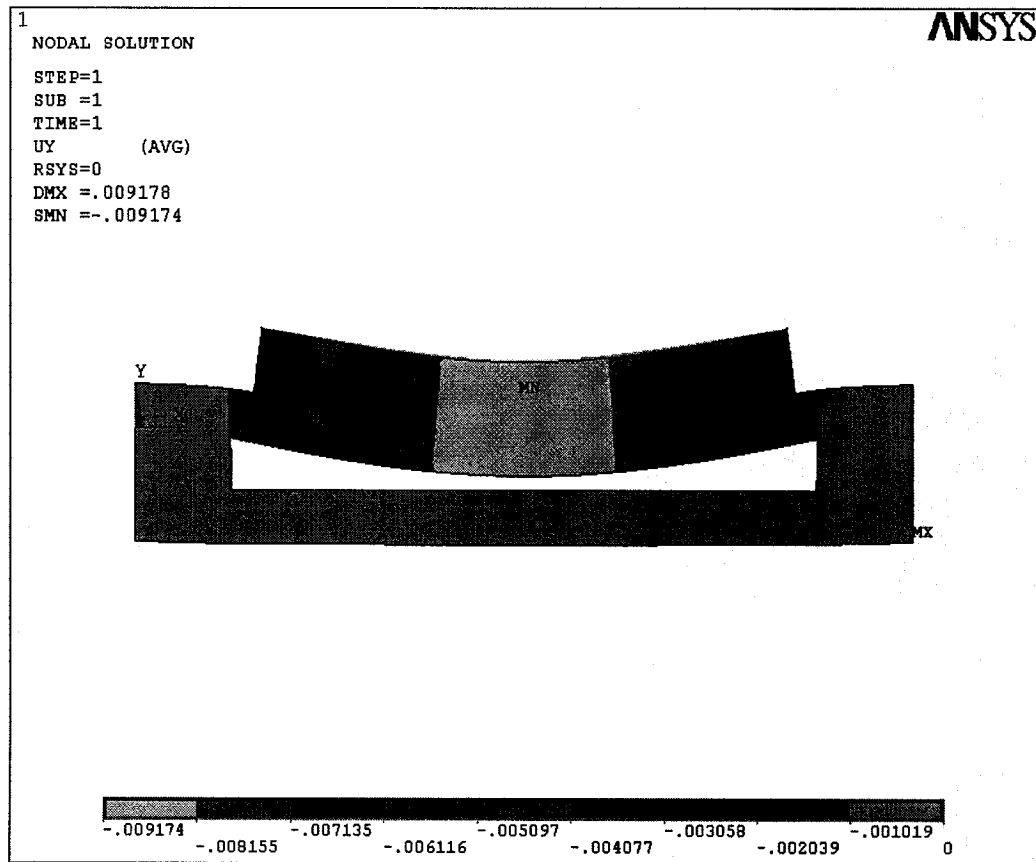
Figure 4-6. Side view of ANSYS model of the displacement of the membrane to an applied
pressure.

Figure 4.6 shows the ANSYS model of the displacement of the membrane when a
pressure of 0.133 N/mm^2 was applied From the figure, it can be seen that the deflection is
maximum at the centre of the membrane.
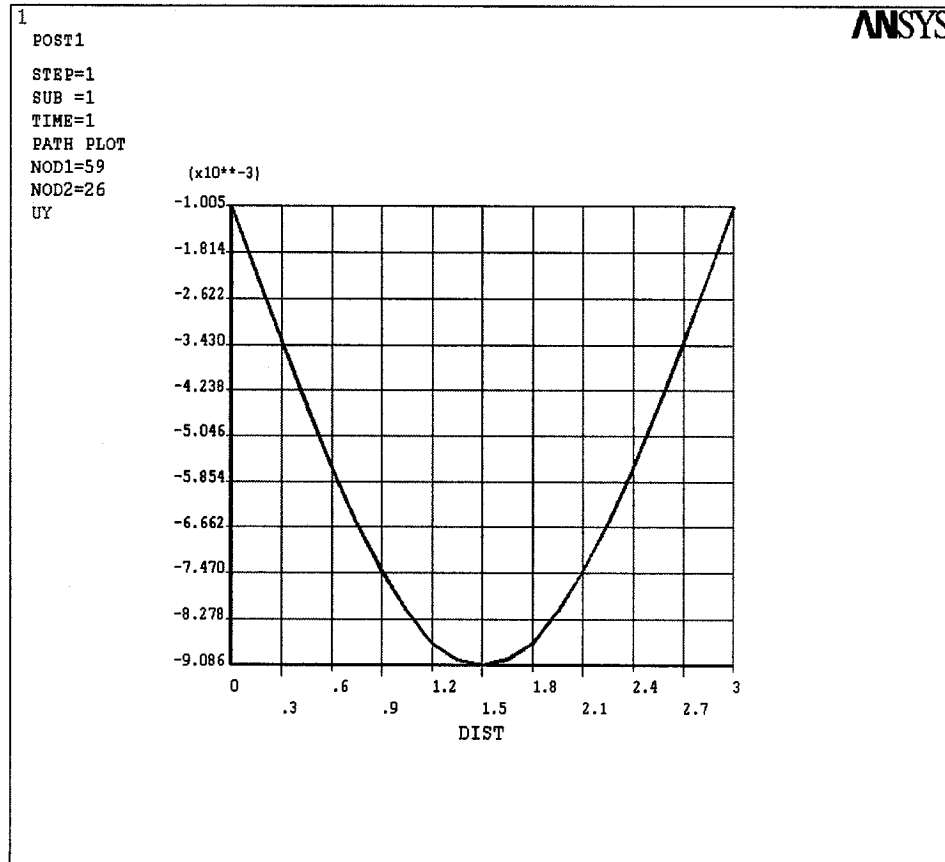
Figure 4-7. ANSYS plot of deflection across the membrane.

A plot (Figure 4-7) of deflection versus the profile of the membrane for an applied pressure of 0.133 N/mm^2 is in agreement with analytical results in Figure 4-3. The deflection on Y-axis and the length of the membrane on X-axis are in mm.

4.5.2 Stress Calculations from ANSYS Model

Stress calculation is an important factor in the design of the tactile sensor and this is obvious from the fact that the membrane has to withstand the pressure applied from the tissue without fracturing. ANSYS was used to find the stress (in N/mm^2)at the junction of the tooth and the membrane where it is maximum. Figure 4.8 shows the contour of the

stress distribution when a pressure of 0.133N/mm^2 is applied on the tooth. The maximum

stress is at the junction where the tooth is fixed to the silicon substrate. Figure 4-9 shows

the plot of the stress versus the membrane geometry.
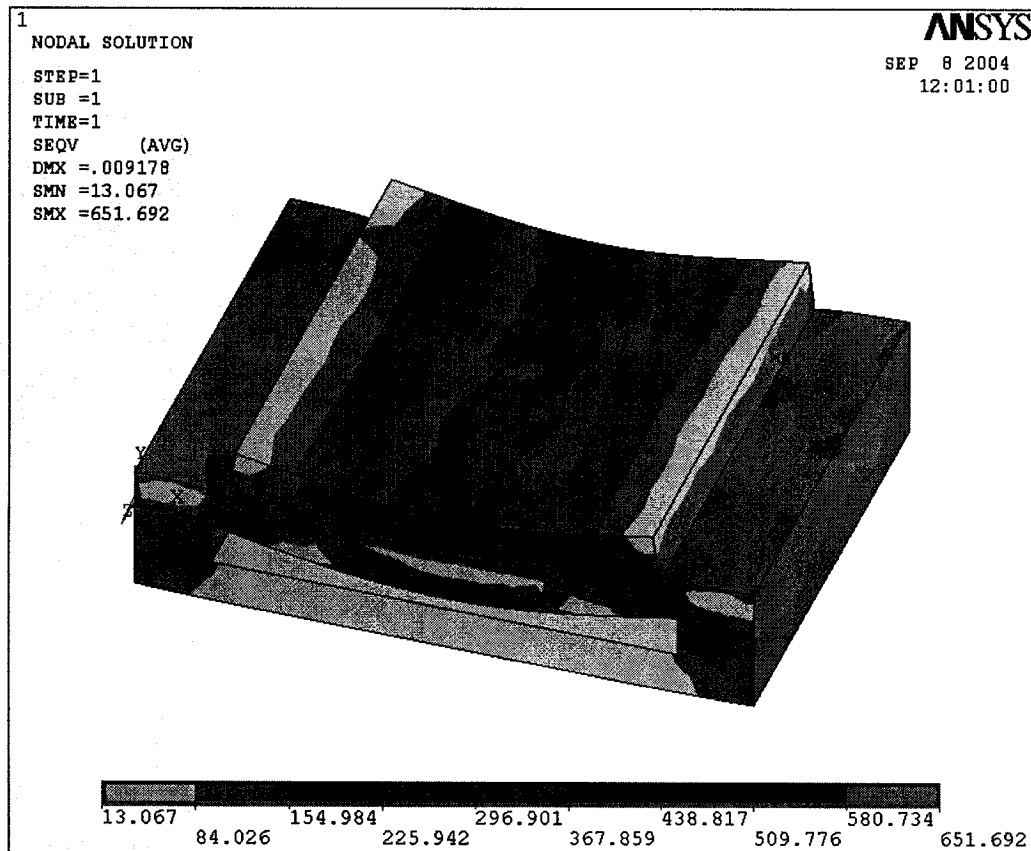
Figure 4-8. ANSYS figure of the stress distribution in the tooth to an applied pressure.
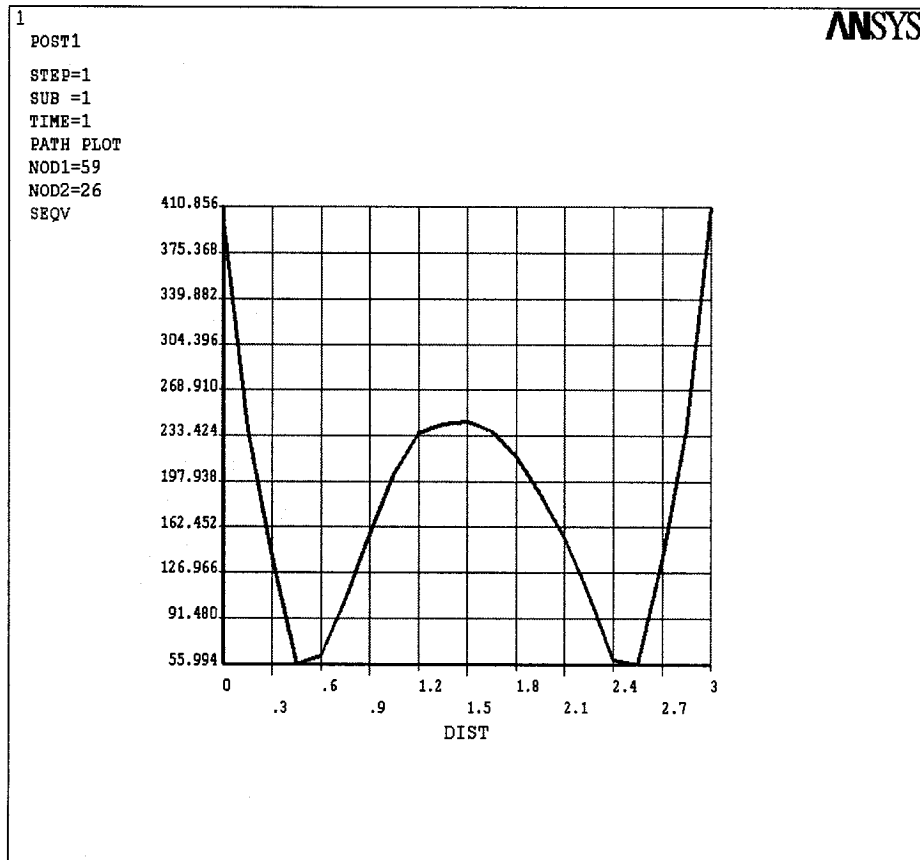
Figure 4-9. Plot of stress versus the membrane geometry.

The stress obtained in Figure 4-9 is in N/mm^2.

4.6 Comparison of the ANSYS and Analytical Model

Figure 4-11 shows the plot of the maximum deflection versus the applied pressure on the tooth for the numerical (ANSYS) and analytical models. From the two plots, it can be understood that both the analytical and numerical models are in good agreement. The deflection on Y-axis is in μm.
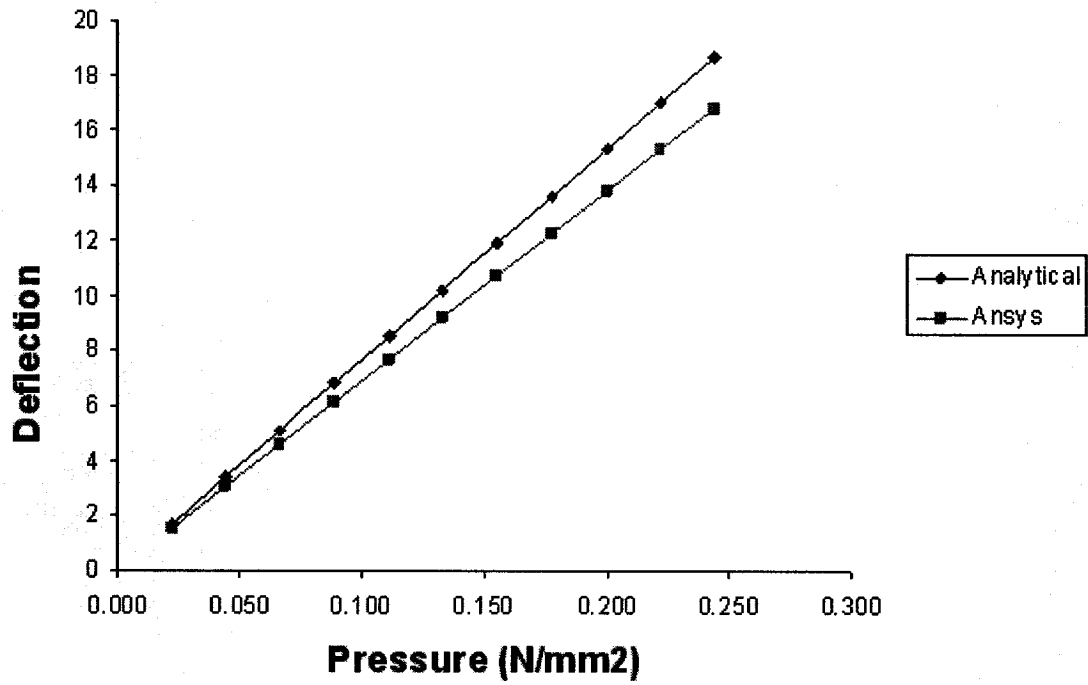
Figure 4-11. Comparison of ANSYS and Analytical model.

The following chapter describes the experiments conducted on the fabricated tactile sensor. Experiments were conducted to study both the static and dynamic response of the sensor.

60

CHAPTER - 5

Experimental Testing and Results

In this chapter the two prototype tactile sensors were experimentally tested for their dynamic and static responses. The schematic and dimensions of the etched cavity on the silicon substrate are shown in the Figure 5-1. Two prototype sensors were made from designs differing in the dimension of the etched cavity on the Silicon substrate. The first design had an etched cavity of 3x3 mm compared to 4x2 of the second design. The characteristic dimension "L" in Figure 5-1 represents the length of the etched cavity. . A photograph of the prototype tactile sensor used in the course of this work is shown in Figure 5-2.
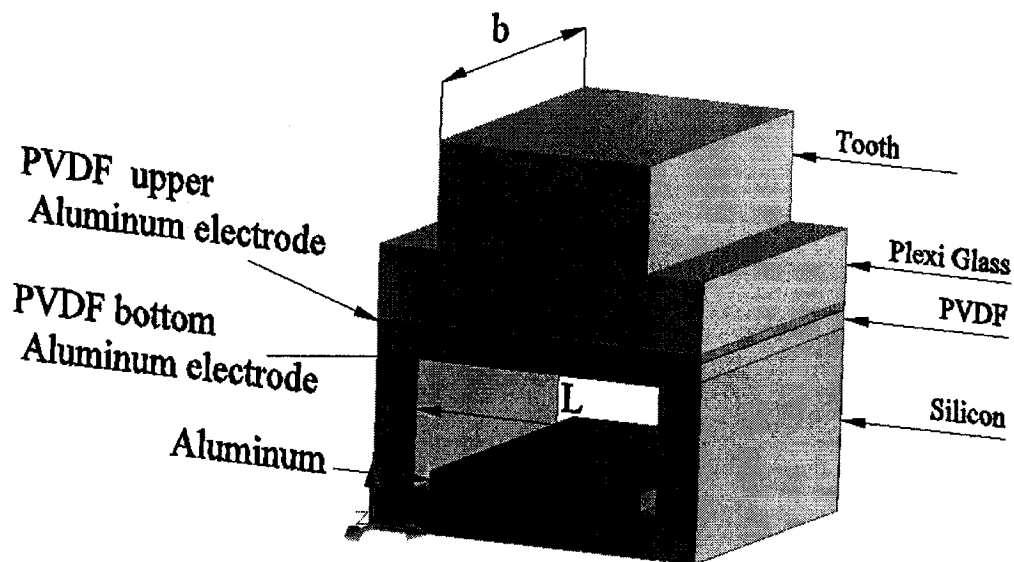
Figure 5-1. Schematic of single tooth prototype tactile tensor.

61

Tooth of the sensor

Base support for the
sensor

Electrodes taken out for
connections

Tooth of the sensor
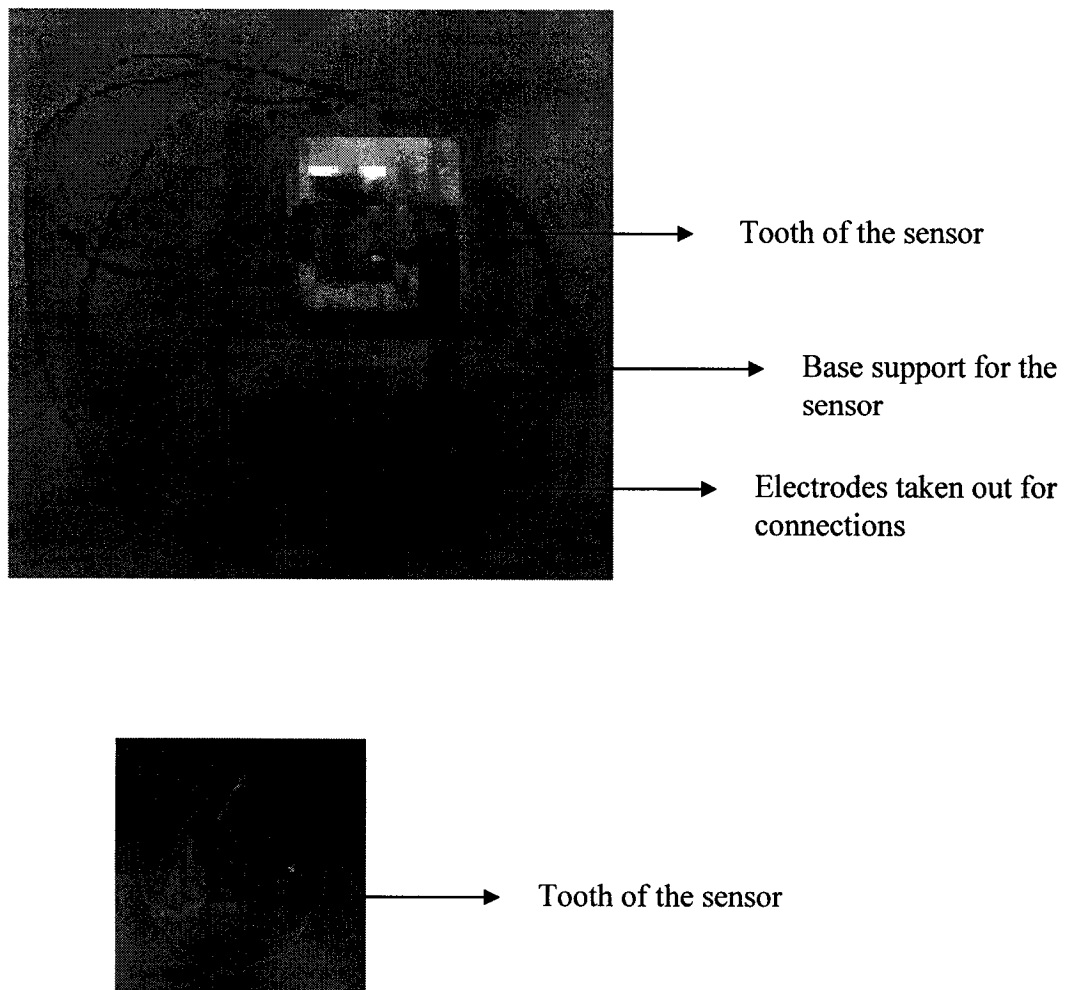
Figure 5-2. A photograph of the prototype tactile sensor

5.1 Experimental Setup

Figure 5-3 shows the experimental setup for testing the tactile sensor. The
designed prototype sensor is capable of measuring both static and dynamic loads.
experiments were done to study both loading conditions.
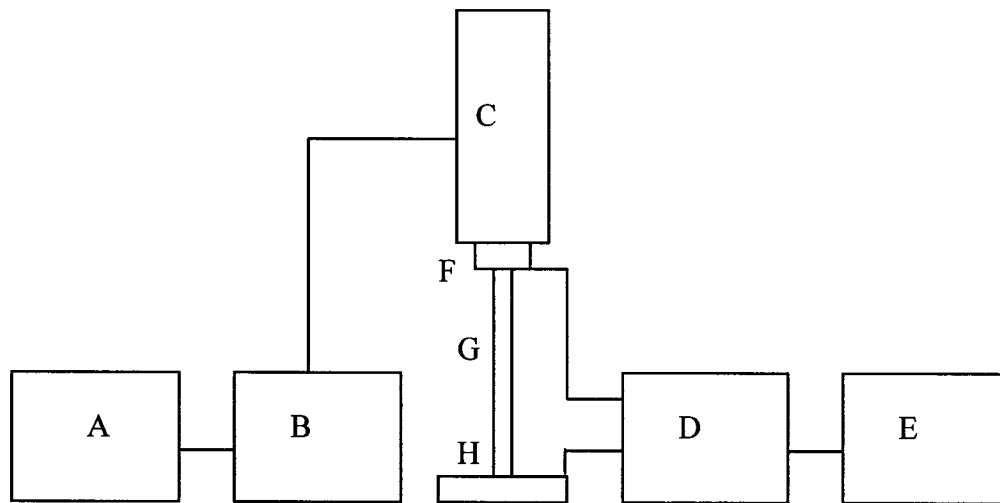
Figure 5-3. Schematic of system for investigating concentrated load on the sensor.

A - Power Amplifier   E - Oscilloscope

B -   Signal generator   F – Force transducer

C -   Vibrator   G – Probe

D - Charge amplifier   H – Tactile sensor

The approach used to investigate the prototype tactile sensor was to apply static load for capacitance output and dynamic load for voltage output. Figure 5.4 shows the experimental setup for testing the tactile sensor. As mentioned earlier, two different designs were tested with the probes used for testing these designs being different. The probes used for testing these designs had the same size as the teeth of the respective sensors. The vibration unit was driven by a signal generator, The probe attached to the vibration unit applied a sinusoidal force (at a frequency of 10Hz) to the sensor for studying its dynamic response.
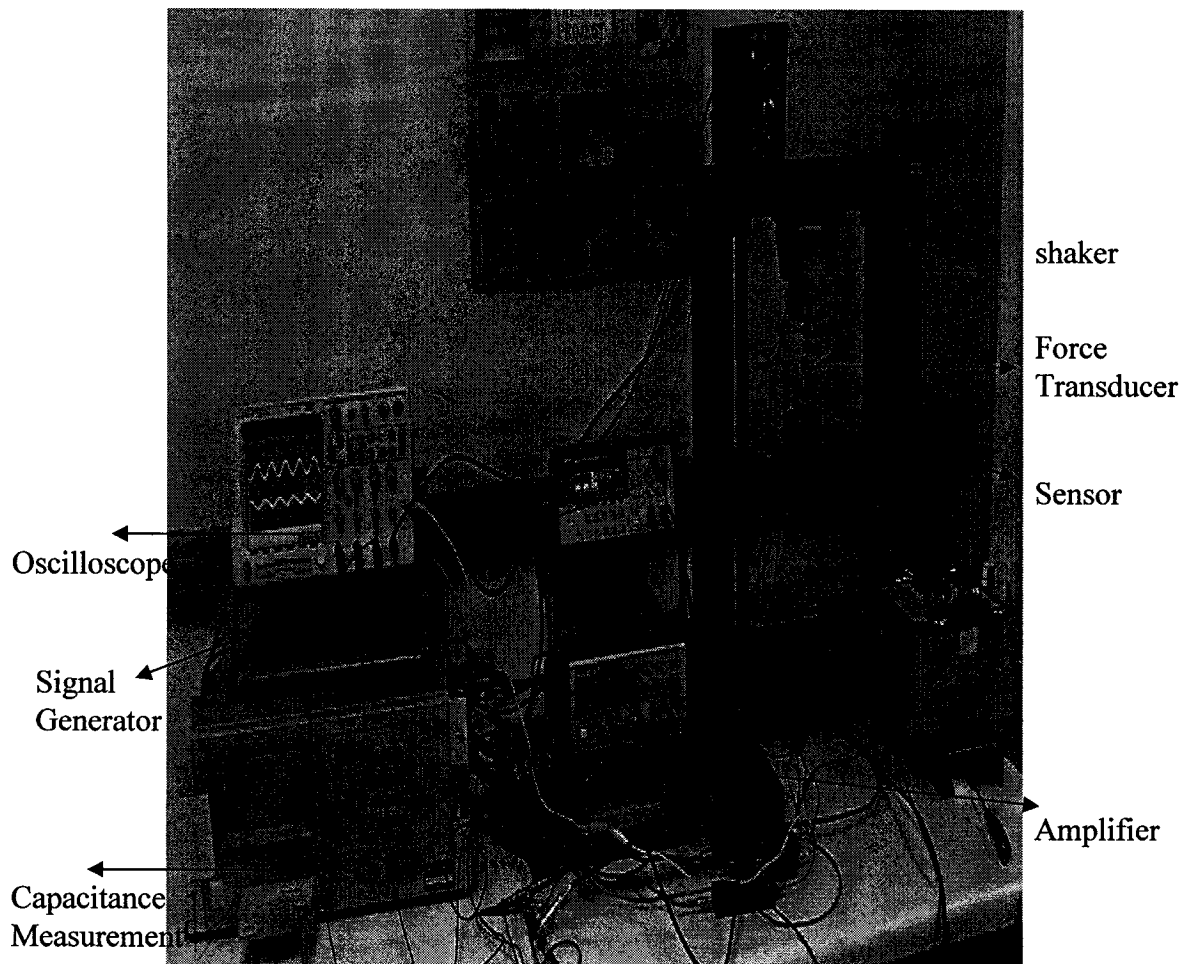
Figure 5-4. Experimental setup for testing the sensor

The voltage output of the PVDF was monitored by a charge amplifier and displayed on an oscilloscope. A force transducer was used to apply a static load directly on the sensor. The observed capacitance output between the bottom electrode of the PVDF film and electrode deposited on the Silicon cavities were measured with the help of a capacitance measurement device. Figure 5.5 shows a load application on the sensor.
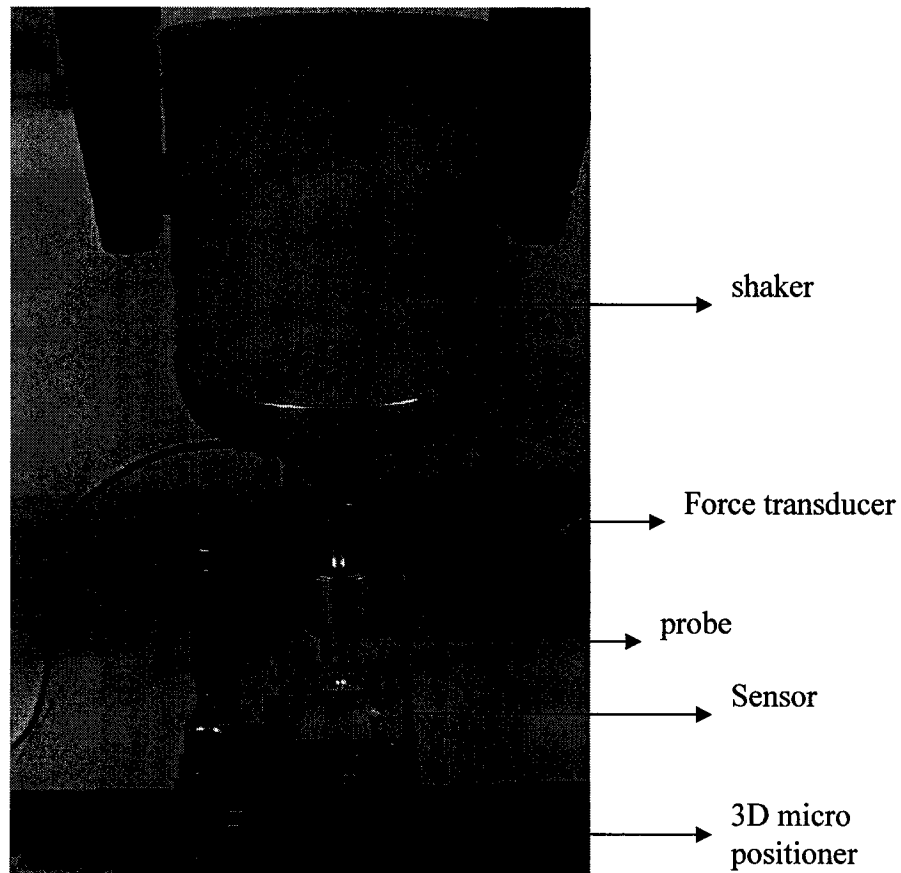
Figure 5-5. Load application on the sensor from the load-cell.

The error from the measurements comes firstly from the positioning of the center of the probe on the center of the intended tooth. Considering the diameter of the probe, a possible mispositioning of 0.05 mm is estimated. Secondly a possible 1-mm variation in extracting the peak values of the sinusoidal trace from the Oscilloscope was estimated. Nonuniform stretching of the PVDF film in gluing to the substrate also introduces additional error. These induced errors were difficult to measure.

5.2 Results

5.2.1 Results obtained for Static Response of the sensor

The following are the sample results from experiments with different loading conditions. To characterize the device, a static load from a load-cell is applied on the top of the teeth of the sensor, as a result of which the intermediate PVDF film is strained. The resultant change in the geometry of the device is reflected in the change in capacitance between the lower electrode of PVDF film and the Al metal deposited in the silicon cavity.
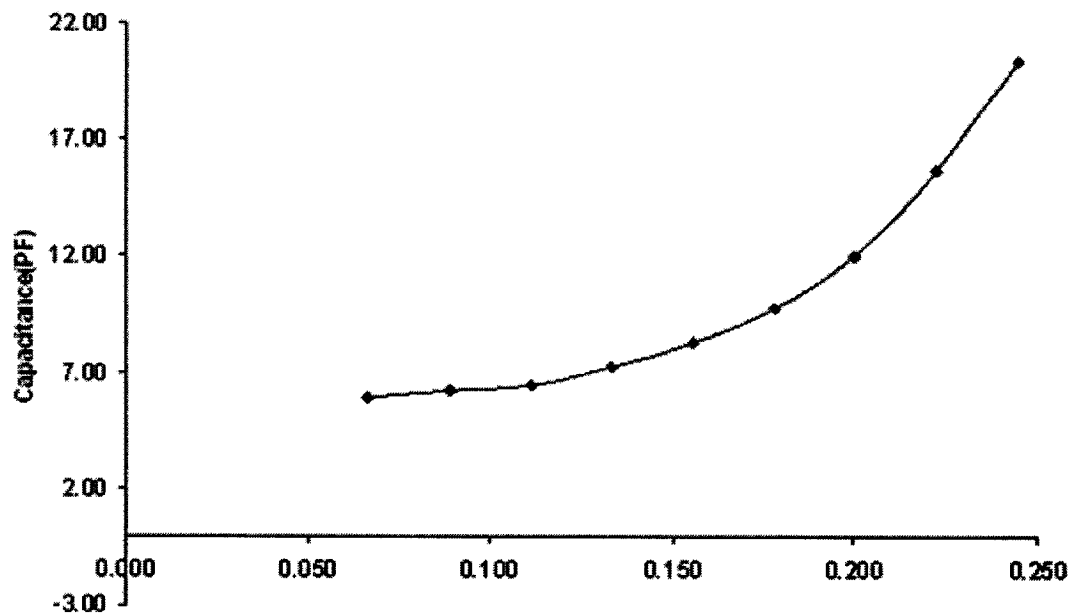
Figure 5-6. Plot of pressure versus capacitance for design-1

From Figure 5-6 (for Design Prototype 1), it can be seen that the capacitance between the lower electrode of the PVDF film and the Al deposited on the silicon cavity increases with the increase in pressure on the teeth of the sensor.
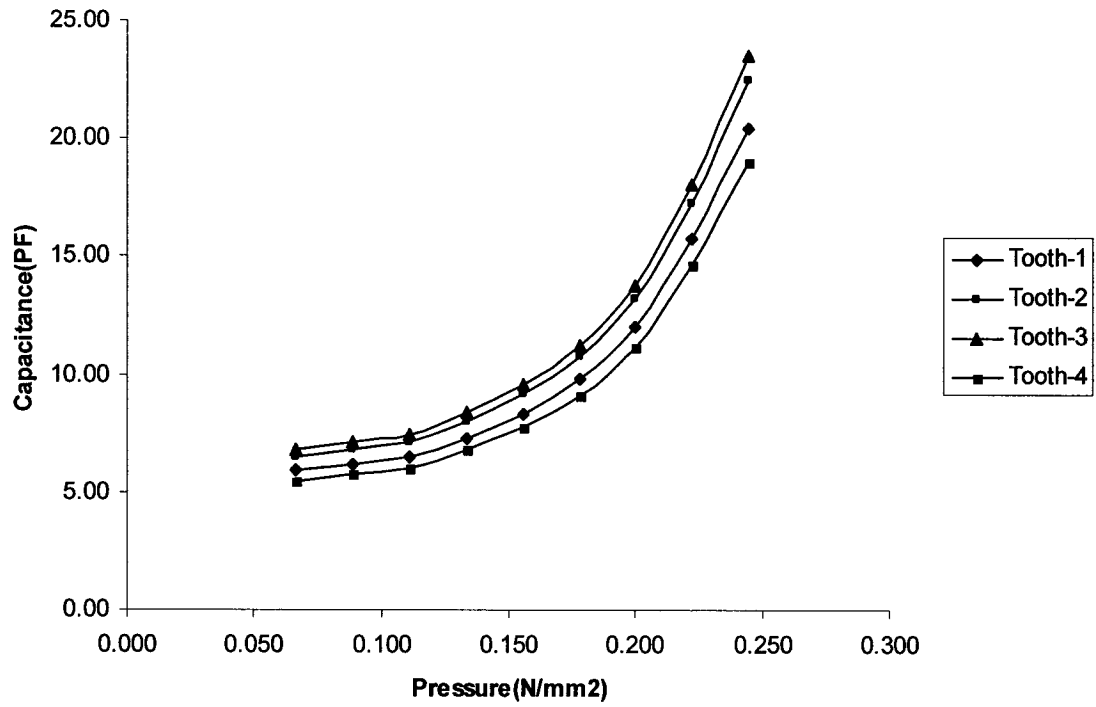
Figure 5-7. plot of pressure versus capacitance for Design-1, For different Tooths

Figure 5-7 shows the plot between the pressure versus the capacitance for the prototype Design-1, when load is applied on the four different tooth of the sensor. It can be seen from the graph that the variations in the capacitance for the same applied pressure on the different tooth of the sensor are almost the same as they are symmetric in structure.

67
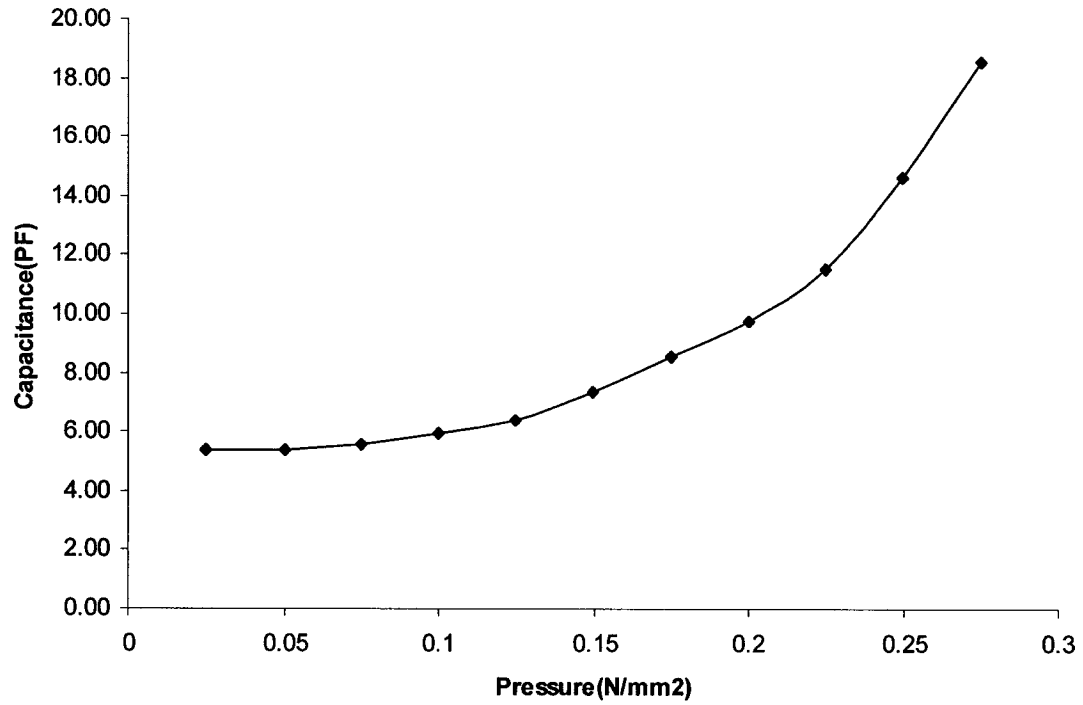
Figure 5-8. plot of pressure versus capacitance for Design-2

As noticed earlier with design prototype 1, prototype 2 also exhibits an increase in capacitance with increasing applied load as shown in Figure 5-8.

Figure 5-9 shows the plot between the applied pressure versus the capacitance for the prototype Design-2, when pressure is applied on the four different tooth of the sensor. It can be seen from the graph that the variations in the capacitance for the same applied pressure on the different tooth of the sensor are almost the same. On comparing the response of a set of any three teeth with the remaining tooth, it was noticed that there was a variation of up to 5 to 15%
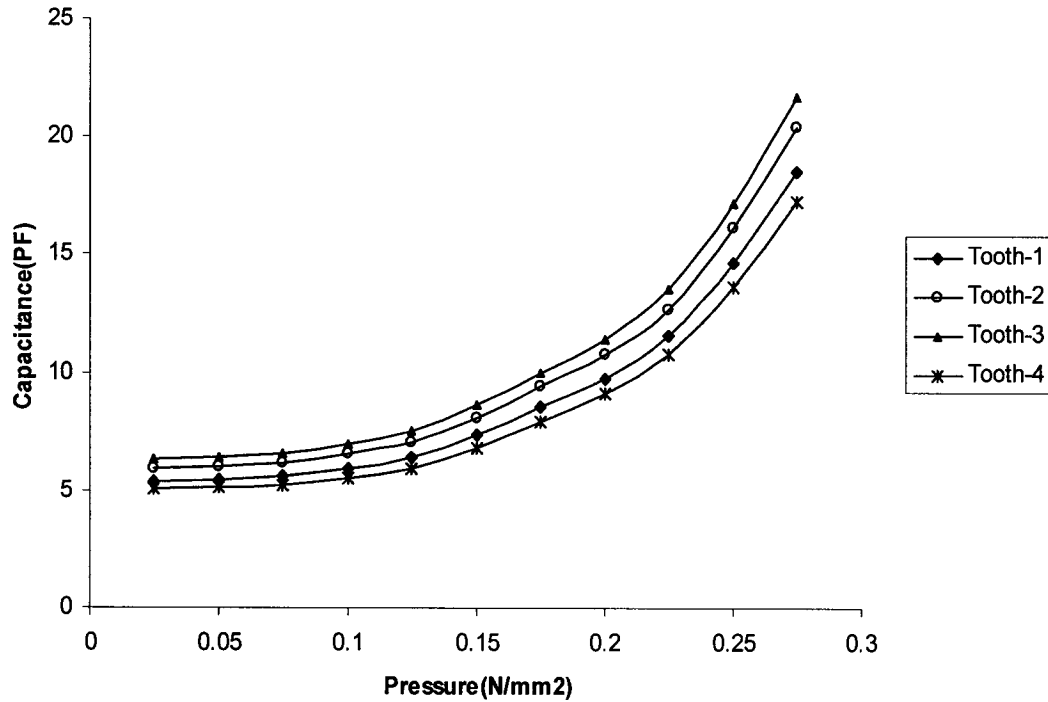
Figure 5-9. Plot of pressure versus capacitance for Design-2, for different Tooths

5.2.2   Results obtained for Dynamic Response of the Sensor

The dynamic response of the tactile sensor was studied by applying a sinusoidal force (at a frequency of 10Hz) on the tooth of the sensor. The magnitude of the dynamic load applied was measured using a load cell. The vertical motion of the teeth leads to the tensile strain in the PVDF film, which, in turn gives rise to a potential difference across the two electrodes of the a PVDF film. This time-dependent potential difference is observed on an oscilloscope. The observed potential difference signal was found to be sinusoidal until an applied pressure of 0.25 N/mm^2. The measured peak-to-peak voltage is plotted against the peak-to-peak value of the applied pressure.
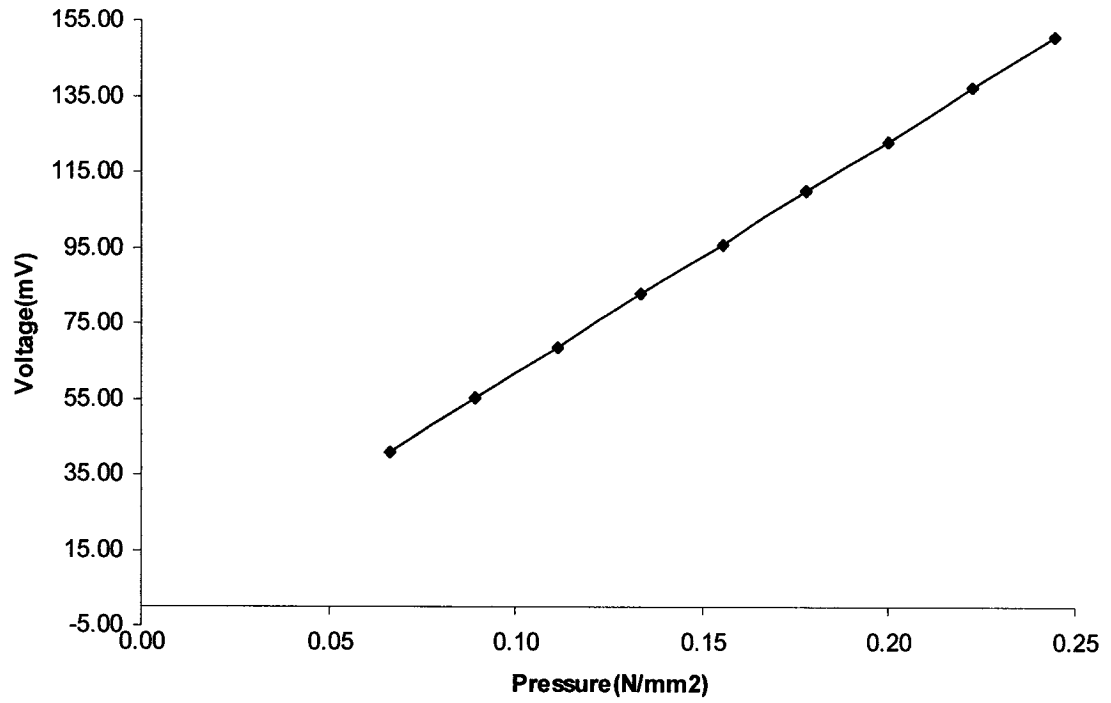
Figure 5-10. Plot of pressure versus peak to peak voltage for Design-1

Figure 5-10 shows the plot of Pressure versus peak to peak voltage output from PVDF film for the prototype Design-1 and pressure applied on tooth-1. It can be seen from the plot that with the increase in pressure on the tooth of the sensor, the peak to peak voltage output from the PVDF film increased linearly .
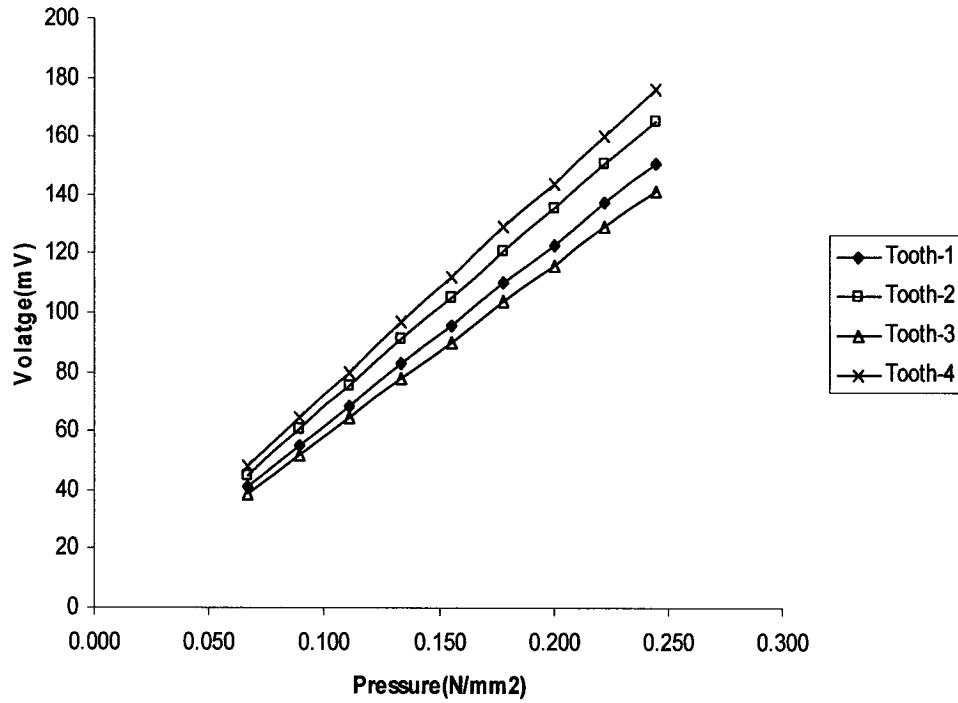
Figure 5-11. Plot of pressure versus peak to peak voltage for Design-1, for different tooths

As observed in the case of static loading, all the teeth of the sensor responded identically to the applied pressure, owing to their similar structures, although the variation in responsively was between 5 to 15% when the response of any set of three teeth was compared to the remaining tooth. A plot depicting the peak to peak voltage output with varying applied pressures for all teeth in design prototype 1 is shown in Figure 5-11.

71
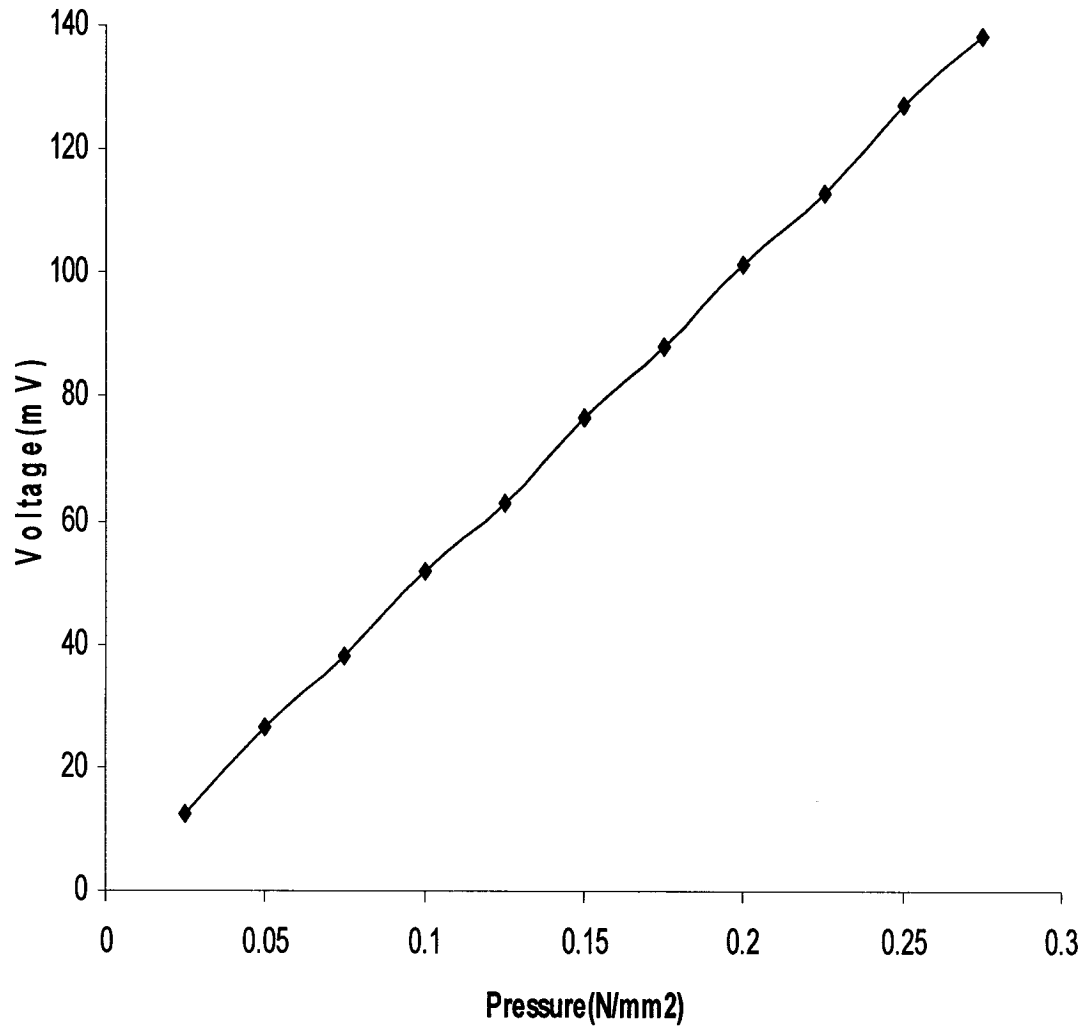
Figure 5-12. Plot of Pressure versus Peak to peak voltage for Design-2, Tooth-1

Figure 5-12 shows the plot of Pressure versus peak to peak voltage output from PVDF film for the prototype Design-2 and load applied on tooth-1. It can be seen from the plot that with the increase in the applied pressure on the tooth of the sensor, the peak to peak voltage output from the PVDF film increased linearly.
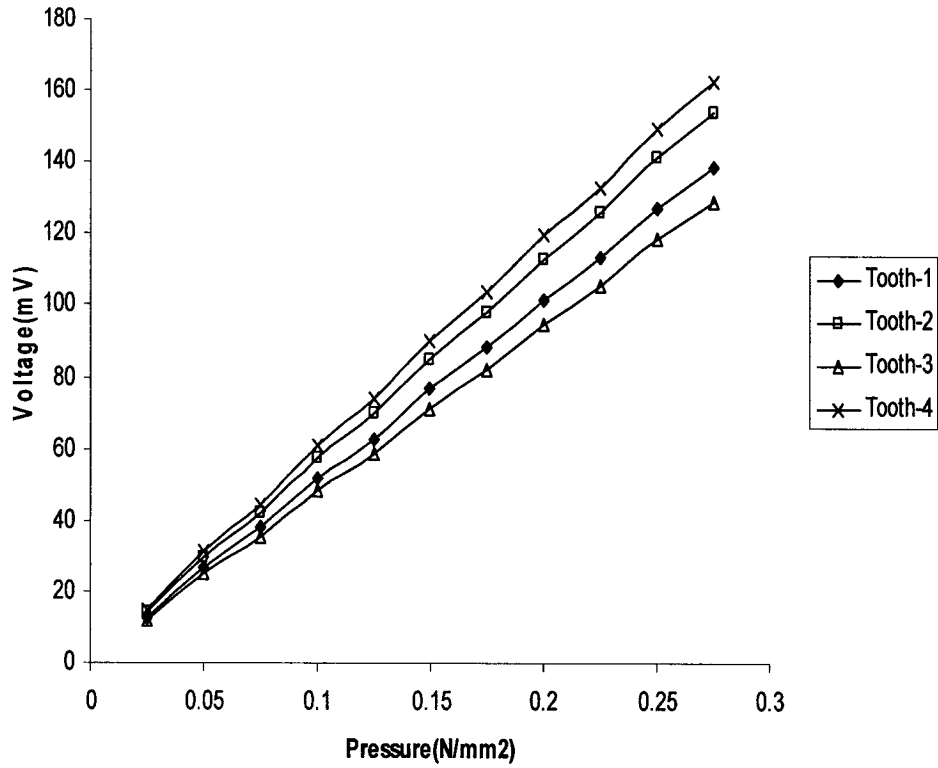
Fig 5-13. Plot of pressure versus peak to peak voltage for Design-2, for different tooth's.

Figure 5-13 shows the plot of Pressure versus peak to peak voltage output from PVDF film for the prototype Design-2 and Load applied on four different teeth. It can be seen from the graph that the variation in the peak to peak voltage output from the PVDF film for the same applied dynamic load on the different teeth of the sensor are identical

5.3   Comparison of the Analytical Model with the Prototype Sensor

Figures 5-14 and 5-15 show plots of pressure versus change in capacitance between the lower electrode of the PVDF film and the Al deposited on the silicon cavity for prototype designs 1 and 2, compared to the results of the analytical model developed

in Chapter 4. A variation of 30% and 22% were observed when comparing the analytical

model results with designs 1 and 2 respectively.
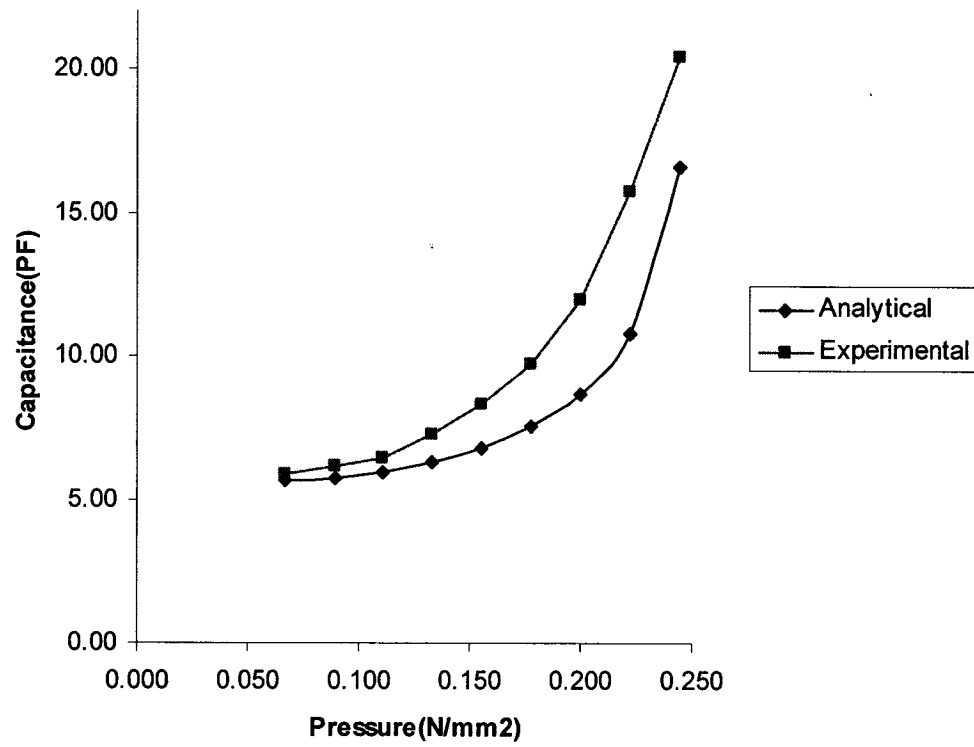
Figure 5-14. Comparison of analytical and experimental results for Design-1
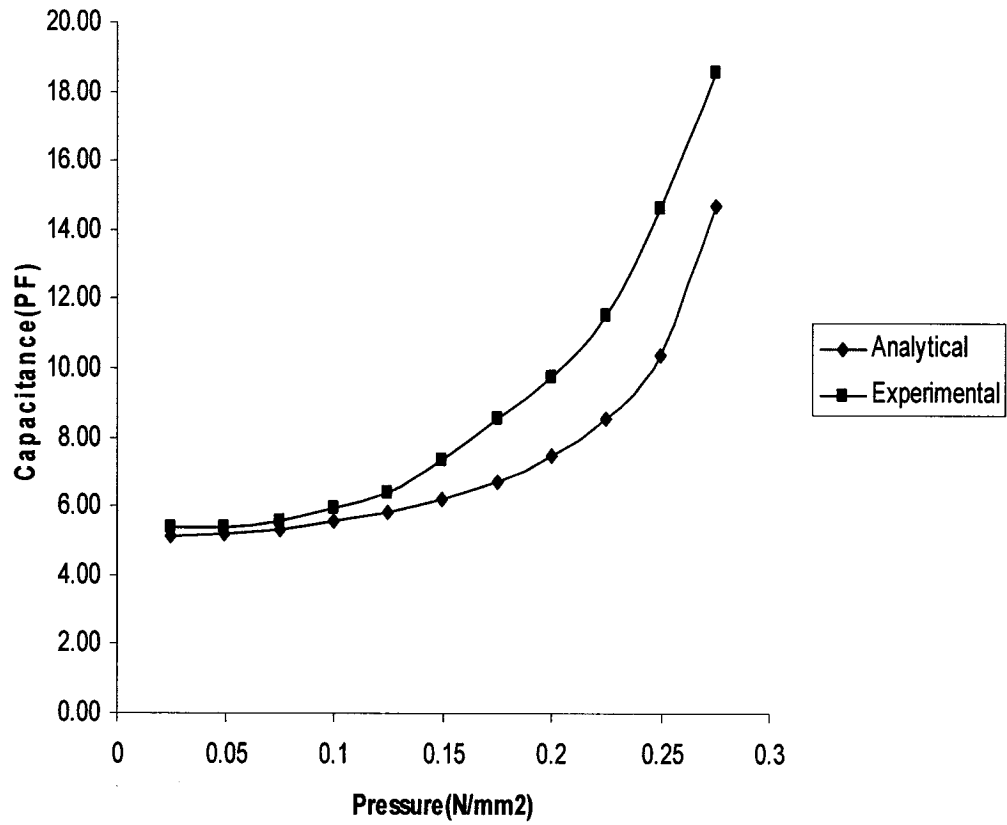
Figure 5-15. Comparison of analytical and experimental results for Design-2

The next chapter presents a discussion of results obtained in this work, followed by conclusions and scope for future work.

CHAPTER - 6

Discussion of Results, Conclusions and Future Work

6.1 Discussions of Results

Mask making is the most crucial step for the design as the entire sensor performance is depending on how accurate mask is made. Extreme care has to be taken while deciding the exposure time and distance of the light source during mask fabrication. The exposure time of 2 to 3 seconds and a distance of 30 cm mentioned in this work was determined after repeated trial and error experiments. Care was also taken while developing the mask until a clear image of the design can be seen on the photosensitive glass.

The size of cavities and electrodes and teeth were determined by the limitations in handling by the equipment in the lab. For example, the hollow cylindrical chamber used for oxidation could not handle samples of sizes greater than 2" x 2". Similarly, the vacuum chuck of the spinner also wasn't capable of handling larger sizes than 2" x 2".

A mask was made to pattern the PVDF film. PVDF films used in this work were available with Aluminum electrode coated on both sides. The sensor design necessitates the patterning of Aluminum on one side of the PVDF film. To accomplish this, the PVDF film was glued to a Silicon substrate using photoresist and was then baked in an oven at 60°C so that the photoresist strongly binded the PVDF and Silicon substrate. Since the PVDF film loose some of it's piezoelectric properties over 70°C, the temperature of the oven was not raised above 60°C. After photolithography, the Silicon wafer attached with

76

the PVDF film was dipped in the aluminum etchant solution. The problem; however with this method is that the etchant tends to penetrate through the bounding between the PVDF film and the Silicon substrate and etches the aluminum film on the underside of the PVDF film. Moreover, the process of separating the PVDF film from the Silicon substrate also has a detrimental effect on the quality of the remaining film on the underside of the PVDF film. To avoid this problem, Aluminum on the PVDF film was patterned by applying the aluminum etchant directly on the PVDF film using a paint brush.

The difference between analytical and experimental results (Figures 5-13 and 5-14) can be attributed to quite a few factors namely:

1. The effect of additional layer of glue to bind the Silicon wafer, PVDF film and Plexiglass was not considered in the analytical model. The addition of glue contributes to a reduction in capacitance owing to an increase in the distance between the adjacent layers (Silicon wafer + PVDF film and PVDF film + Plexiglass). Incorporating this aspect in the analytical model might help in reducing the difference with experimental results.

2. Analytical model for measuring capacitance was constructed using a 1-D premise while in reality, the structure is 3-D. This assumption contributed significantly to the differences observed between the experimental and the theoretical results.

3. As mentioned in section 3.7, aligning of each component with respect to the other during assembly are crucial in realizing a near-ideal tactile sensor

77

performance. Limitations encountered during the fabrication process have contributed to the discrepancies observed.

6.2 Conclusions

A silicon micromachined tooth-like tactile sensor that is suitable for integrating with the tip of a grasper of an endoscopic surgical instrument was developed. Device operation was studied for both static and dynamic response during grasping based on the change in capacitance between the aluminum electrode of the PVDF film and aluminum electrode , deposited inside 20 µm deep cavities etched in silicon and output from the piezoelectric effect of the 25 µm thin PVDF film respectively. The range of load applied was from 0.067 N/mm^2 up to 0.244 N/mm^2 using a rectangular probe of 3mm by 3mm. This was within the limitation of human tactile sensing during minimally invasive surgery. Since the device has a tooth-like surface at its top, it is possible to integrate it with an endoscopic surgical instrument.

Further development to the present work will yield a sensor that can be incorporated into a surgical device for providing the surgeon with a sense of touch.

6.3 Future Work

6.3.1 Packaging

Various issues have to be addressed for sensors that are designed to function inside the human body. One of the primary concerns for such type of sensors is

compatibility with bodily fluids. The tactile sensor developed has to be packaged in such a way that the bodily fluids do not come into contact with the PVDF film and the connecting wires. Also the rest of the sensor should be able to withstand the attack of the corrosive fluids in the body. Hence the sensor needs to be encapsulated.

6.3.2 Robustness and Reliability

The proposed tactile sensor for endoscopic surgery with the 25μm membrane is suitable for feeling pulses in arteries or veins, in that the sensor does not experience considerable stress or force. But the tactile sensor would not be suitable for grasping thick or harder tissues. A possible solution would be to increase the depth of the cavity for the sensor to withstand larger loads. But at the same time the issue of sensitivity has to be kept in mind since increasing the depth would decrease its sensitivity.

6.3.3 Fabrication Techniques for patterning of PVDF and Plexiglass

Patterning of PVDF film and Plexiglass is the most important factor to get the exact output from the designed tactile sensor. Hence, new fabrication techniques have to be applied in order to obtain accurate results.

REFERENCES

1. Melzer, A., Buess, G., Cuschieri, A.,"Instruments and Allied Technology for Enoscopic surgery", Operative Manual of Endoscopic surgery 2, springer-Verlag, New York, pp. 1-69, 1994.

2. Satava, R., "High tech srgery: Speculations on future directions in Minimally Invasive Surgery", McGraw-hill, Inc, 1993.

3. Faraz, A., Payandesh, S., "Engineering Approaches to Mechanical and Robotic Design for Minimally Invasive surgeries ", Kluwer Academic publishers, 2000.

4. Guilak, F., Sato, M., Stanford, C. M., Brand, R. A., "Editorial – Cell Mechanics", Journal of Biomechanics 33, pp.1-2, 2000.

5. Breown, T.,"Techniques for Mechanical Stimulation of cells in vitro: a Review", Journal of Biomechanics 33, pp. 3-14, 2000.

6. Dario, P., Guglielmelli, E., Allotta, B., Carrozza, M. C., "Robotics for medical application", IEEE Robot. Automat. Mag; Vol. 3, pp. 44-56, Sept 1996.

7. Dario, P., Carrozza, M. C., Allotta, B., Guglielmelli, E., "Micromechatronics in medicine", IEEE/ASME Trans. Mechatron; Vol.1, pp. 137-148, june 1996.

8. Taylor, R. H., Lavallee, S., Burdea, G. C., Mosges, R., Eds; Computer-Integrated surgery: Technology and clinical Applications. Cambridge, MA: MIT Press, 1996.

9. Voges, U., "Technology in Laparoscopy - what to expect in the future", Urology Ausgabe (a) 35:208 -14, 1996.

10. Despont, M., "A comparative study of bearing designs and operational environments for harmonic side-drive micromotors", In: proc. of MEMS, pp. 171-176, 1992.

11. Pennypacker, H. S., Iwata, M. M., "MammaCar: A case history in behavioral medicin", in D. Blackman and H.Lejune, eds; Bhaviour Analysis in Theory and pratic:

Contributions and Controversies, East Sussex, UK: Lawrenc Erlbaum Associate Ltd; pp. 259-288, 1990.

12. Phillips, J. R., Johnson, K. O., "Tactile spatial resolution. A Continuum mechanics model of the skin predicting mechanoreceptor responses to bar, edges, and gratings", Journal of Neurophysiology, 46: 1204-1225, 1981.

13. Johansso, R. S., Vallbo, A. B., "Tactile sensory coding in the glabrous skin of the human hand", Trends in Nurosciences, 69(1): 27-32, 1983.

14. Srinivasan, M. A., LaMotte, R. H., "Tactile discrimination of shape: Responss of slowly and rapidly adapting mechanorcepive afferents to a step indented into the monkey fingerpad", journal of Neuroscience, 7(6): 1682-1697, 1987.

15. Fearing, R.S., Cohn, M. B., "Tactile feedback for teleoperation", In: Telemanipulator technology, SPIE Proc., Boston, pp. 641-6, Nov 1992.

16. Metha, M., "A Micromachined Capacitative pressure sensor for use in Endoscopic surgeryRY", M.Sc THESIS, Simon Fraser University, Canada, 1996.

17. Gray, B.L., Fearing, R.S., "A surface micro machined micro tactile sensor array", in proc. IEE. Int. conf. in Robotics and Automation; Mineapolis, MN,pp.1-6, 1996.

18. Drgahi, J., Parameswaran, M., Payandesh, S., "Micro machined piezoelectric tactile sensor for use in Endoscopic Graspers". Int. conf. Intelligent Robots and systems, Proceedings, IEEE/RSJ Vol: 3.p.p:1503-1508, 1998.

19. Bicchi, A., Canepa, G. D., Lacconi, D., "Sensorized Minimally Invasive surgery Tool for detecting Tissual Elastic properties", proc. IEE. Int.conf. Robotics and Automation. Minneapolis, Minnesta, p.p.884-888, 1996.

20. Howe, R. D., "Tactile sensing and control of robotic manipulation", Journal of Advanced Robotics vol.8 no. 3, pp. 245-261, 1994.

21. Fisher, H., Neislus, B., "Tactile Feedback for Endoscopicsurgery", Interactive Technology and New paradigm for health care. IOS Press, pp. 114-117, 1995.

22. Fearing, R. S., "Tactile sensing mechanisms", International Journal of Robotics Research, 9(3):3-23, 1990.

23. Pawluk, D. T. V., Son, J. S., Wellmn, P. S. , Peine, W.J., "A Distributed pressure sensor for Biomedical Measurements", Journal of Biomechanical Engineering 102(2):302-305, 1998.

24. Begej, J., "Planar and finger-shape optical sensors for robotic applications", IEEE J. of Robotics and Automation, 4(5):472-484, 1998.

25. Howe, R. D., "Tactile Sensing and Control of robotic manipulation", Journal of Advanced Robotics, 8(3):245-261, 1994.

26. Dario, P., Bergamsco, M., "An Advanced Robot System for Automated Diagnostics Tasks Through Palpation", IEEE Transactions on Biomedical Engineering, 35(2):118-126, 1988.

27. Maria, C. C., Eisinberg, A., Menciassi, A., Campolo, D., Micer, S., Dario, P., "Towards a force-controlled microgripper for assembling biomedical microdevices", Journal of Micromechanics and Microengineering, pp. 271-276, 2000.

28. Sugiyama, S., Kawahata, K., Yoneda, M., Igarashi, I., "Tactile image detection using a 1K-element silicon pressure sensor array Sensors Actuator", A: 22, pp. 397-400, 1989.

29. Beebe, D. J., Hsiesh, A. S., Denton, D., Radwin, G., "A Silicon force sensor for robotics medicine", Sensors and Actuator A: 50, pp. 55-56, 1995.

30. Gray, B. L., fearing, R. S., "A Surface micromachined microtactile sensor array", Proc.1996 IEEE Int. Conf. On Robotics and Automation, pp 1-6, 1996.

31. Leineweber, M., Pelz, G., Schmidt, M., Kappert, H., Zimmer, G., "New Tactile Sensor chip with silicone rubber cover Sensors Actuators", A: 84, pp. 36-45, 2000.

32. Kolesar, E. S., Dyson, C. S., "object imaging with a piezoelectric robotic tactile sensor", Journal of Microelectromechanics, Syst. 4, pp. 87-96, 1995.

33. Reston, R. R., Kolesar, E. S., "Robotic tactile sensory array fabricated from a piezoelectric polyvinylidene fluoride film", Proc. IEE NAECON Vol. 3, pp 1139-44, 1990.

34. Ando, S., Shinoda, H., "Ultrasonic emission tactile sensing", IEEE Control Syst. Mag. 156, pp. 1-9, 1995.

35. Shimizu, T., Shikida, M., Sato, K., Itoigawa, K., "A new type of tactile sensor detecting contact force and hardnes of an object", proc. IEEE Conf. On MEMS Vol 1, pp 344-347, 2002.

36. Zhang, H., So, E., "Hybrid resistive tactile sensing", IEEE Trans. Syst. Man Cybern. B 32, pp. 57-65, 2002.

37. Jiang, F., Tai, Y. C., Wlsh, K., Tsao, T., Lee, G. B., Ho, C. M., "A flexible MEMS technology and its first application to shear stress sensor skin", Proc. IEEE. Int. Conf. On MEMS, pp. 465-470, 1997.

38. Beebe, D. J., Denton, D. D., "A flexible polyimide-based package for silicon sensors", Sensors Actuators, A 44, pp. 57-64, 1994.

39. Cao, L., Kim, T. S., Zhou, J., Mantell, S. C. , Polla, D. L., "Calibration technique for MEMS memberane type strain sensors", Proc. IEEE Symp. On Microelectronics, pp. 204-210, 1999.

40. Jonathan, E., Jack, C., Chang, L., Bruce, R., "Development of polyimide-based Flexible Tactile Sensing Skin", Mat. Res. Soc. Symp. Proc. Vol. 736 @ Materials Research Society.

41. Kane, B. J., Cutkosky, M. R., Kovarcs, T. A., "A traction stress sensor array in high-resolution robotic tactile imaging", Journal of Microelectromech. Syst. 9, pp.425-434, 2000.

42. Shinoda, H., Ando, S., "Ultrasonic emission tactile sensor for contact localization and characterization", IEEE International conference on Robotic and Automation, proc. 1994.

43. Teramoto, K., Watanable, K., "Acoustical tactile sensor utilizing multiple reflections for principal curvature measurement," SICE. Proc. of the 40th SICE Annual conf. International session papers, 2001.

44. Dargahi, J., "A Piezoelectric tactile sensor with three sensing elements for robotics endoscope and prosthetic application", Sensor and Actuators, Vol. 80, pp. 23-30, 2000.

45. Petter, E., Biehl, M., Meyer, J., " Vibrotactile palpation instrument for use in Minimal invasive surgery", Engineering in Medicine and Biology society, Bridging Disciplines for Biomedicine. Proc. of the 18th Annual International Conf. of IEEE, 1996.

46. Ryan, A., Beasley, T., Robert, D., "Tactile Tracking of Arteries in Robotic Surgery" International Conf. on Robotic & Automation, proc. of IEEE. Washington, DC, May2002.

47. Youngping, Z., Arthur, F., Mak, T., " Effective Elastic properties for Lower Limb Soft Tissues from Manual Indentation Experiment", IEEE Transactions on rehabilitation Engineering, Vol. 7. N). 3, September 1999.

48. MDizaji, M., Dizaji, R. M., " Detection of internal displacement of tissues in ultrasound images using image registration technique", IEEE CCECE, Canadian conference, 2002.

49. Picinbono, G., Delingette, H., Ayache, N., "Nonlinear and anisotropic elastic soft tissue models for medical simulation" proc. ICRA. IEEE , 2001.

50. Gladilin, E., Zachow, S., Deuflhard, P., Hege, H., "A biomechanical model for soft tissue simulation in craniofacial surgery" International workshop on Medical Imaging and Augmented Reality, shatin, hong kong, china, 2001.

51. Scalari, G., Eisinberg, A., Menciassi, A., Carrozza, M. C., Dario, P., "Micro Instrumentation for non-invasive measurement of mechanical properties of tisues", Microtechnologies in medicine and biology, 1st Annual International, conf. Lyon, France pp.199 – 202, 2000.

52. Sumi, C., Suzuki, A., Nakayama, K., " Estimation of shear modulus distribution in soft tissue from strain distribution" IEEE Transaction on Biomedical Engineering, pp. 193-202, Feb 1995.

53. Tritto, G., Pirlo, G., Tritto, M. C., "Soft tissues expanders: computer- assisted simulation of elastic mesh deformation and fractal vascular geometries in controlled skin expansion", Engineering in Medicine and Biology Society, Images of the Twenty-First Century. Proc. of the Annual International Conf. of the IEEE Engineering in Seattle, WA Vol. 6, pp. 1951-1952 , 1989.

54. Brouwer, I., Jeffrey, U., Loren, B., Alana, S., Neel, D., Frank, T., "Measuring In Vivo Animal Soft Tissue Properties for Haptic Modeling in Surgical Simulation", Eds, IOS Press, pp. 69-73, 2001.

55. Vacalebri, P., Lazzarini, R., Roccella, S., Vecchi, F., Carrozza, M . C., Zecca, M., Dario, P. D., " A Robotic system for soft Tissue Characterization".

56. Klaesner, J. W., Commean, P. K., Hastings, M. K., Zou, D., Mueller, M. J., " Accuracy and reliability testing of a portable soft tissue indentor", IEEE Transactions on Neural Systems and Rehabilitation Engineering. VOL.9, Issue-2, pp. 232-240, Jun 2001.

57. Yun. C, "Deflection of beams for spans and cross sections", McGraw-hill, Inc, 1986.

58. Cady, W.G., "Piezoelectricity", 1st ed., McGraw-Hill Inc., New York, 1946.

59. Toupin, R.A., "A Dynamical theory of elastic dielectrics," International Journal of Engineering Science, Vol. 1, pp. 101-126, 1963.

60. Toupin, R.A., "The Elastic dielectric," Journal of Rational Mechanical Analysis, Vol. 5, No. 6, pp. 849-915, June 1956.

61. Tiersten, H.F., "Coupled magneto mechanical equations for saturated insulators," Journal of Mathematical Physics, Vol. 5, No. 9, pp. 1298-1318, 1964.

62. Allik, H., Hughes, T.J.R., "Finite element method for piezoelectric vibration", International Journal for Numerical Methods in Engineering, Vol. 2, pp. 151-157, 1970.

63. Peelamedu, S., Naganathan, G., Barnett, A., Rao, D. " Finite element approach to model and analyze piezoelectric actuators", American Institute of Aeronautics and Astronautics (AIAA) Journal, Feb 1999.

64. Peelamedu, S., Niemeyer, S., Naganathan, G., Rao, D., "Piezoceramic array actuator system for deformable mirror applications", Journal of Smart Materials and Structures, Dec 1999.

APPENDIX - A

Piezoelectric Effect

Piezoelectric substances are new materials used for sensor and actuators with the help of micro electromechanical systems technology. When external force is applied to piezoelectric materials it generates charge on the surface, which is proportional to applied mechanical stress. The converse effect is also there, applied voltage generates deformation in the materials. Similarly ferroelectric type of material is one which exhibits a spontaneous polarization in one or more direction of the crystal over a definite temperature range. Piezoelectric must not be confused with the Ferro electricity, which is the property of a spontaneous or induced electric dipole moment. All ferroelectric materials are piezoelectric, but the contrary is not always true. Piezoelectricity relates to the crystalline ionic structure. Ferro-electricity instead relates with electron spin.

A simplified model of piezoelectricity entails the motion of anions (-) and cations (+) moving opposite directions under the influence of an electric field and mechanical force. The force generated by this motion cause lattice deformation for non-Centro symmetric crystals due to presence of both high and low stiffness ionic bonds. As results, all piezoelectric materials are anisotropic, in case of central symmetry; an applied force does not yield an electric polarization. The effect for quartz is shown below in Figure A.1, positive and negative charges are formed. It is important to remember that the piezoelectric materials are function of the continuously changing mechanical deformation. Therefore dynamic forces are used in practical situations.
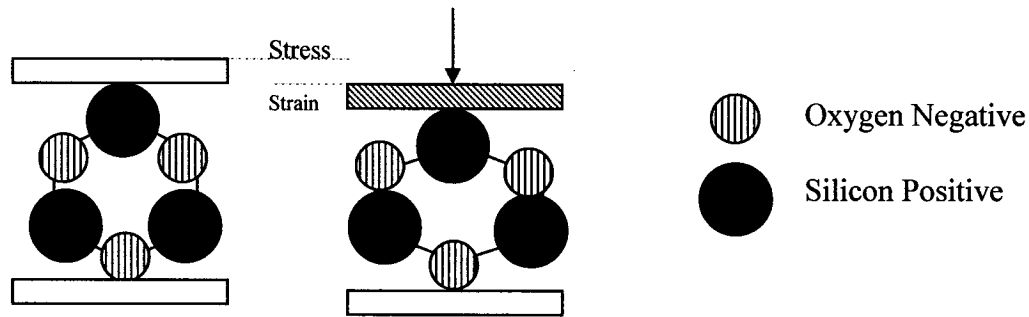
Figure A.1 Piezoelectric in ionic crystals such as quartz, ion position in quartz lattice with and without applied stress.

A.1 Piezoelectric Materials

The most extensively used natural piezoelectric materials are crystals (quartz and tourmaline). In synthetic piezoelectric, ceramics formed by many tightly compacted monocrystals (1μ in size) are most popular. These Ceramics, such as Lead Zirconate titanate (PZT), barium titanate is ferroelectrics. To align the dipoles to monocrystals in same direction, they are subjected to strong electric field during their manufacturing process. The applied electric field to crystal above the Curie temperature to align the dipoles. Then cool the crystal while maintaining the field. This process makes crystal permanent electric polarized. When electric field is removed, the crystalline cannot reorder in random from because of mechanical stresses accumulated, resulting in permanent electric polarization. The problem with these materials relates to their temperature sensitivity and aging when approaching the curie temperature.

Polymers such as polyvinylidene fluoride (PVDF), also display piezoelectric properties and have pyroelectric features, i.e. change the electrical charge with change in temperature. PVDF are not central symmetry i.e. it display piezoelectric properties.

Compared to quartz and ceramics, piezo-film is more pliant and lighter in weight. In addition to this it is rugged, inert and low cost. Secondly urethane and epoxy adhesive are used for gluing PVDF. The use of epoxy and urethane adhesives depends upon the strength requirement of the structure.

In smart structures, piezo ceramics are typically used as actuators, polymeric piezoelectric materials are typically tactile sensor, temperature and stain sensors. It is common practice to embed piezoelectric sensors into prototypes because these sensors can be manufactured with strength and dimensional characteristics that do not degrade the structural integrity of the material from which the prototype device is made. Piezoelectric ultrasonic motors and piezoceramic sensors are currently being built into commercial products such as camera lens drives and automotive engine control systems. In many cases, thin layers of piezoceramic composites are bonded to other structural material surfaces. When thermal effects are generated through either friction or direct exposure to significant temperature gradients, the reliability of the electrode layer in these piezoceramics can completely dominate the performance of the device.

Many efforts have been done for mathematical modeling of piezoelectric phenomenon. The researcher efforts in piezoelectricity carried out in the past produced in our work. Cady [58], gave comprehensive description of development in the theory of piezoelectricity. Toupin [59-60], involved in development of the governing equation using energy methods and dynamics theory. Tiersten [61], made several approximations and developed linear equation of piezoelectricity using Hamiltonian mechanics and variation techniques. Allik and Hughes [62], developed the general equation of motion

for piezoelectric materials in a matrix form. The S. Peelamedu [63-64], combined the work together to formulate finite element solution for piezoelectric structure.

Basic Constitutive Equations [61] are expressed in matrix notation as

$$[T] = [c]\{S\} - [e]^T\{E\}$$
$$[D] = [e]\{S\} + [\varepsilon]\{E\}$$

(A1.1)

The first and second equation represents structural and electrical constitutive of piezoelectric material, respectively. Where as the entire matrix are given as

{T} = Stress vector (N/m^2)

{D} = Electric flux density (C/m^2)

{E} = Electric Field Vector (V/m)

{S} = Strain vector (dimensionless)

[c] = Elasticity Matrix (N/m^2)

[e] = Piezoelectric matrix at constant stress(C/m^2)

[ε] = Dielectric Matrix

A.2   Piezoelectric Coefficients

Most of piezoelectric coefficients have double subscript that links electrical and mechanical quantities. The first subscript gives the direction of the electrical field associated with voltage applied and second subscript gives the direction of the mechanical stress or strain.

90

A.2.1 D - Coefficients

The piezoelectric constant relating the mechanical strain produced by an applied electric field are termed the strain constant or 'd' coefficients or piezoelectric strain matrix. Conversely the coefficient may be viewed as relating the charge collected on the electrodes, to the applied mechanical stress. The unit of 'd' coefficient is C/N.

$$d = charge\ density/applied\ mechanical\ stress.$$

A.2.2 E – Coefficients

The piezoelectric constant relating the electrical field produced by applied mechanical stress at constant strain is known as stress constant or 'e' coefficient or piezoelectric stress matrix. The unit of 'e' coefficient is C/m^2 There is relationship between [e] and [d] matrix and it is given as

$$[e] = [d]\ [c] \tag{A1.2}$$

For 3D analysis Z-axis are considered as polarized axis and size of array [e] and [d] is 6x3. If we are considering the 2D analysis then we use Y- axis as polarized axis and order of array [e] and [d] is 4x2. Similarly for $[\varepsilon]$ matrix size are different for 3x3 and 2x2 for 3D and 2D model respectively.

A.2.3 G Coefficients

The piezoelectric constants relating the electric field produced by a mechanical stress are termed the voltage constants, or the "g" coefficients. The units are then expressed as volts/meter per Newton/square meter.

$$g = \frac{Electric\,Field}{Applied\,Mechanical\,Stress} \qquad\qquad (A1.3)$$

High g_{ij} constants favor large voltage output, and are sought after for sensors. The relationship between the [d] and [g] matrix is given as

$$[d] = [K]^{T}[g] \qquad\qquad (A1.4)$$

A.2.4 Dielectric Constants

The relative dielectric constant is ratio of the permittivity of material, ε, to the permittivity of free space, ε_{o}, in the unconstrained condition.($\varepsilon_{o} = 8.9 \times 10^{-12}$ farad/meter).

$$K = \frac{Permittivity\,of\,materail}{Permittivity\,of\,free\,space} = \frac{\varepsilon}{\varepsilon_{o}} \qquad\qquad (A1.5)$$

A.2.5 Capacitance

Capacitance is a quantity dependent on the type of materials and its dimensions. Unit of capacitance is Farad. Capacitance is expressed by following formula

$$C = \frac{K\varepsilon_{o}A}{t} \qquad\qquad (A1.6)$$

where as 'A' area of electrodes, 't' is gap between the electrodes.

A.2.6 Young's Modulus

Young's Modulus is ratio of stress (force per unit area) to strain (change in length per unit length). Unit of young Modulus is N/m^{2}.

$$Y = \frac{Stress}{Strain} \qquad\qquad (A1.7)$$

92

A.2.7 Density

The ratio of the mass to volume in the material, expresses in Kg/m^3

$$\rho = \frac{mass}{volume}$$

<div align="right">(A1.8)</div>

A.2.8 Curie Temperature

The Temperature at which the crystal structure changes from a non-symmetrical (piezoelectric) to a symmetrical (non- Piezoelectric)form, expresses in degrees Celsius.

A.2.9 Pryoelectricity

Piezoelectric materials are also pryoelectric. They produce electric charge as they undergo a temperature change. When their temperature is increased, a voltage develops having the same orientation as polarization voltage. The change in electric field due to a temperature change is given as.

$$E_{pyro} = \frac{\alpha \Delta T}{K_3 \varepsilon_o}$$

<div align="right">(A1.9)</div>

where as, E is the induced electrical field (volts/meter), α is the pyroelectric coefficient in Coulomb/$^0Cm^2$, ΔT is temperature difference in ^0C.

A .3 Analytical Approach

The analytical method is demonstrated in this section. In this section relation between the voltage generation and force applied are discussed. The force F is applied to the rectangular piezoelectric plate of size L x T x W. The Figure A.2 demonstrates the

working of the rectangular piezoelectric plate. The voltage and charge develop by this force is given as

$$Q = F \, d_{33} \qquad\qquad\qquad (A1.10)$$

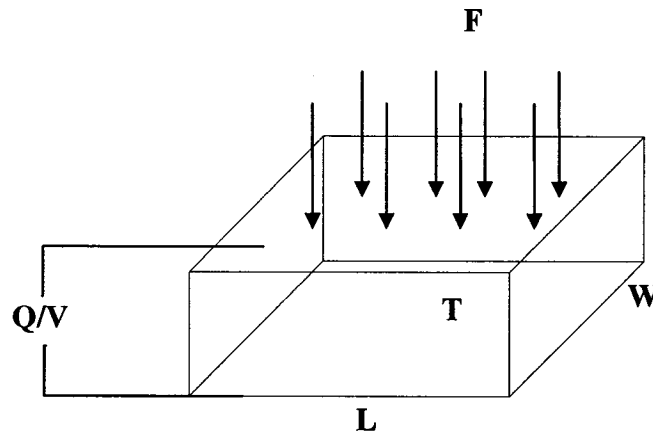$$\frac{V}{T} = \frac{Fg_{33}}{LW} \qquad\qquad\qquad (A1.11)$$

Figure A.2 Voltage generation by the piezoelectric substance

APPENDIX - B

ANSYS Finite Element Listings

Finite element modeling is a numerical method of solving engineering and mathematical physics problems in the areas of structural analysis, heat transfer, fluid flow, mass transport and electromagnetic potential, involving complicated geometries, loadings and material properties.

Analytical solutions are given by mathematical expression that yields the value of the desired unknown quantities at any location in a body. These analytical solutions generally require the solution of ordinary or partial differential equations. Which in case of the complex geometries, loading and material properties are not usually obtainable. Hence, numerical methods such as the finite element method, which formulates a system of simultaneous algebraic equations rather than requiring the solution of complex differential equations, are employed for acceptable solutions. Finite Element Analysis makes it possible to evaluate a detailed and complex structure, in a computer, during the planning of the structure. The demonstration in the computer of the adequate strength of the structure and the possibility of improving the design during planning can justify the cost of this analysis work. FEA has also been known to increase the rating of structures that were significantly over designed and built many decades ago. In the finite element method, a structure is broken down into many small simple blocks or elements. The behavior of an individual element can be described with a relatively simple set of

equations. Just as the set of elements would be joined together to build the whole structure, the equations describing the behaviors of the individual elements are joined into an extremely large set of equations that describe the behavior of the whole structure. The computer can solve this large set of simultaneous equations. From the solution, the computer extracts the behavior of the individual elements. From this, we can get the stress and deflection of all the parts of the structure. The stresses will be compared to allowed values of stress for the materials to be used, to see if the structure is strong enough. This type of modeling a body is called as discretization.

The term "finite element" distinguishes the technique from the use of infinitesimal "differential elements" used in calculus, differential equations, and partial differential equations. The method is also distinguished from finite difference equations, for which although the steps into which space is divided are finite in size, there is little freedom in the shapes that the discreet steps can take. Finite element analysis is a way to deal with structures that are more complex than can be dealt with analytically using partial differential equations. FEA deals with complex boundaries better than finite difference equations will, and gives answers to "real world" structural problems. It has been substantially extended in scope during the roughly 40 years of its use. Finite Element Analysis makes it possible to evaluate a detailed and complex structure, in a computer, during the planning of the structure. The demonstration in the computer of the adequate strength of the structure and the possibility of improving the design during planning can justify the cost of this analysis work. FEA has also been known to increase the rating of structures that were significantly overdesigned and built many decades ago.

In the absence of Finite Element Analysis (or other numerical analysis), development of structures must be based on hand calculations only. For complex structures, the simplifying assumptions required to make any calculations possible can lead to a conservative and heavy design. A considerable factor of ignorance can remain as to whether the structure will be adequate for all design loads. Significant changes in designs involve risk. Designs will require prototypes to be built and field tested. The field tests may involve expensive strain gauging to evaluate strength and deformation. With Finite Element Analysis, the weight of a design can be minimized, and there can be a reduction in the number of prototypes built. Field testing will be used to establish loading on structures, which can be used to do future design improvements via Finite Element Analysis.

This research employs the commercial finite element analysis package ANSYS. This software was used to construct an element model of the tactile sensor. This model was used to predict the deflection of the PVDF and Plexi-glass membrane under an applied pressure. The operations performed in Ansys are explained in the flowchart below. Ansys can be used in two different modes either in programming mode or in graphical mode. The graphical mode is much user friendly and the problems can be solved step by step. The flow chart is given in the Figure B-1, demonstrate the approach of the ansys step by step.
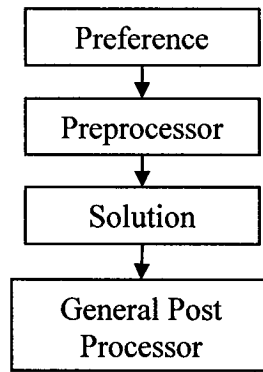
```
┌─────────────────┐
│   Preference    │
└─────────────────┘
         │
         ▼
┌─────────────────┐
│  Preprocessor   │
└─────────────────┘
         │
         ▼
┌─────────────────┐
│    Solution     │
└─────────────────┘
         │
         ▼
┌─────────────────┐
│  General Post   │
│   Processor     │
└─────────────────┘
```

Figure B-1 The Flow chart of step by step general approach in Ansys.

Preference

The first step of solving the model in Ansys is to describe the type and method of analysis. In our case we used structural analysis with h-method.

Preprocessor

This is main body of modeling the problem and defining the element type, materials properties and real constant. In this section first we defined the element type and its materials properties. The selection of the element is main process in modeling. The modeling and meshing was performed in next step. The following are the main operation performed in the Preprocessor, shown in Figure B-2.
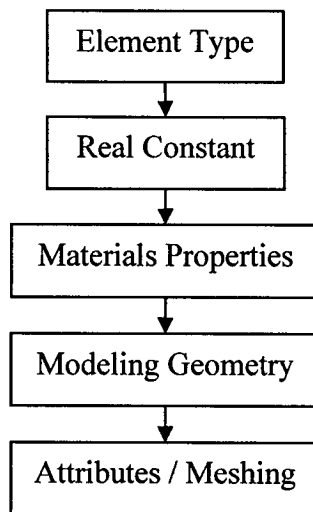
98

Figure B-2 Flow Chart of processes in the Preprocessor section

Solution

In this section of ansys solution of modeled problem is carried out. The first part is to define analysis type such as static, harmonic, dynamic etc. In loads section loads and boundary conditions are applied to the model. The last step is to solve the meshed model. The flow chart is presented in the Figure B-3.
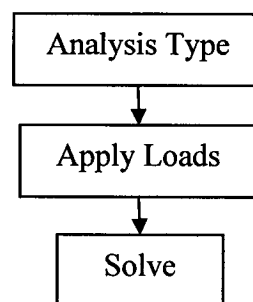
FigureB-3 Flow chart of Solution Section

99

General Post Processor

In this section of the ansys results are reviewed after the solving the problem in solution section. There are many options available to see the results. Plot section and list section provide the results in the graphical presentation and numerical values, respectively. Any results such as stresses, strains, reactions at any point can be visualized with the help of graphical section.

ANSYS 6.0 Input listing for deflection of the Membrane

```
Input Listing for the 3-D Model
/BATCH
!/menu,on
/FILNAM
/TITLE,design
/UNITS,USER
/PREP7
MSHKEY,0
MSHAPE,1,3d
FLST,5,3,6,ORDE,3
FITEM,5,1
FITEM,5,3
FITEM,5,-4
CM,_Y,VOLU
VSEL, , , ,P51X
CM,_Y1,VOLU
CHKMSH,'VOLU'
CMSEL,S,_Y
!*
VMESH,_Y1
!*
CMDELE,_Y
CMDELE,_Y1
CMDELE,_Y2
!*
/VIEW,1,1,1,1
/ANG,1
/REP,FAST
FINISH
```

```
/SOL
!*
ANTYPE,0
FLST,2,2,5,ORDE,2
FITEM,2,23
FITEM,2,25
!*
/GO
DA,P51X,ALL,0
FLST,2,2,5,ORDE,2
FITEM,2,20
FITEM,2,22
!*
/GO
DA,P51X,UY,0
FLST,2,1,5,ORDE,1
FITEM,2,21
/GO
!*
SFA,P51X,1,PRES,5/3
/STATUS,SOLU
SOLVE
FINISH
/POST1
/EFACE,1
AVPRIN,0, ,
!*
PLNSOL,U,Y,0,1
/VIEW,1,,,1
/ANG,1
/REP,FAST
```

APPENDIX - C

Interfacing with Electronics

C.1   Capacitance of Piezo Sensor

To use a piezoelectric material as a sensor, it is necessary to make device for measuring its surface charge. One such method consists of sandwiching a piezo between two metal plates to make a capacitor. Metalized PVDF films are available in the market aluminum coated on the both sides as shown in Figure C-1.
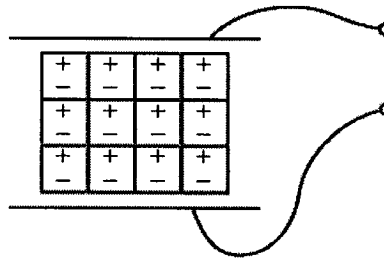

Figure C-1. PVDF Film act as Capacitor with Aluminum Coating

An applied force will produce a voltage $V = Q_f / C$, where Q_f is the charge resulting from the force and C is the capacitance of the device. The electrical equivalent circuit for this sensor is shown in Figure C-2
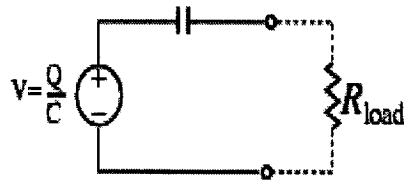
Figure C-2. Electrical Equivalent Circuit for Sensor

The voltage source represents the voltage that develops due to excess surface charge on the crystal. The capacitor represents the metallic plates. The load resistance results from the act of measuring the voltage across the terminals. Piezo sensors are only useful for measuring dynamic forces, as the capacitance blocks direct current.

C.2. The Role of Load Resistance

The most critical part of an interface circuit is the load resistance. Figure C-3 shows a load resistance that is connected to both sides of piezo film electrodes. The load resistance affects low frequency measurement capability as well as the signal amplitude. It also effects circuit in terms of time constant, loading effect, and frequency response.
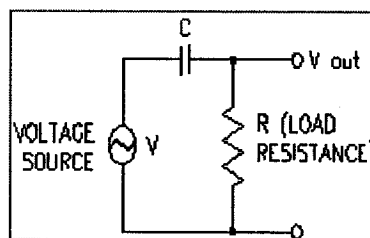

Figure C.3. Purpose of Load Resistance

C.3 Charge Amplifier and Voltage Amplifier

Two type of circuit used for the amplification of the piezoelectric sensor. Both the amplification circuit has advantages and disadvantages depending upon application. This amplification can be as charge mode amplification and voltage mode amplification. Both circuits configuration of the charge amplifier and voltage amplifier are shown in the Figure C-4.
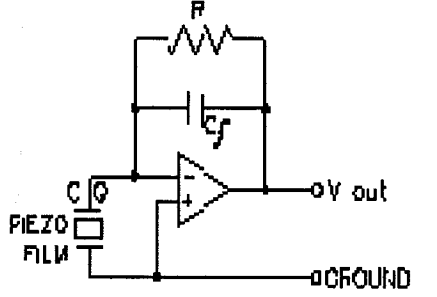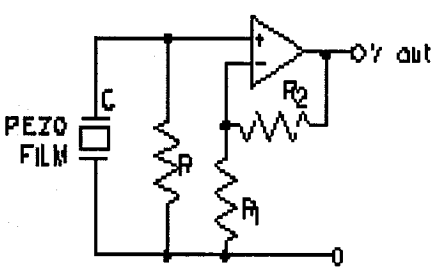
Charge Amplifier	C_f = Feed Back Capacitance $V_{out} = C/C_f$ Voltage Gain = C/C_f Time constant = R C_f
Voltage Amplifier	Voltage Gain = $1 + R_1/R_2$ Time Constant = RC

Figure C-4. Charger Amplifier and Voltage Amplifier

The main advantage of charger amplifier exists while using of electronic circuit at distance from the sensor. It also minimizes the charger leakage. On the other hand voltage amplifier shows less dependence on the temperature. The charger amplifier was used for signal amplification in our case.

104